

Anatomy of $B \rightarrow D\bar{D}$ Decays

Lennaert Bel^a, Kristof De Bruyn^a, Robert Fleischer^{a,b},
Mick Mulder^a and Niels Tuning^a

^a*Nikhef, Science Park 105, NL-1098 XG Amsterdam, Netherlands*

^b*Department of Physics and Astronomy, Vrije Universiteit Amsterdam,
NL-1081 HV Amsterdam, Netherlands*

Abstract

The decays $B_d^0 \rightarrow D_d^- D_d^+$ and $B_s^0 \rightarrow D_s^- D_s^+$ probe the CP-violating mixing phases ϕ_d and ϕ_s , respectively. The theoretical uncertainty of the corresponding determinations is limited by contributions from penguin topologies, which can be included with the help of the U -spin symmetry of the strong interaction. We analyse the currently available data for $B_{d,s}^0 \rightarrow D_{d,s}^- D_{d,s}^+$ decays and those with similar dynamics to constrain the involved non-perturbative parameters. Using further information from semileptonic $B_d^0 \rightarrow D_d^- \ell^+ \nu_\ell$ decays, we perform a test of the factorisation approximation and take non-factorisable $SU(3)$ -breaking corrections into account. The branching ratios of the $B_d^0 \rightarrow D_d^- D_d^+$, $B_s^0 \rightarrow D_s^- D_d^+$ and $B_s^0 \rightarrow D_s^- D_s^+$, $B_d^0 \rightarrow D_d^- D_s^+$ decays show an interesting pattern which can be accommodated through significantly enhanced exchange and penguin annihilation topologies. This feature is also supported by data for the $B_s^0 \rightarrow D_d^- D_d^+$ channel. Moreover, there are indications of potentially enhanced penguin contributions in the $B_d^0 \rightarrow D_d^- D_d^+$ and $B_s^0 \rightarrow D_s^- D_s^+$ decays, which would make it mandatory to control these effects in the future measurements of ϕ_d and ϕ_s . We discuss scenarios for high-precision measurements in the era of Belle II and the LHCb upgrade.

Contents

1	Introduction	1
2	Decay Amplitudes and Observables	2
2.1	Amplitude Structure	2
2.2	CP-Violating Asymmetries	3
2.3	Untagged Decay Rate Information	6
2.4	Information from Semileptonic Decays	7
3	Picture Emerging from the Current Data	10
3.1	Overview	10
3.2	Preliminaries	10
3.3	Comparing $B \rightarrow D\bar{D}$ Branching Fractions	11
3.3.1	Probing Annihilation Topologies with Charged B decays	12
3.3.2	Probing Exchange and Penguin Annihilation Topologies	14
3.3.3	Probing Exchange and Penguin Annihilation Topologies Directly	17
3.4	Global Analysis of the Penguin Parameters	21
3.4.1	Information from Branching Ratios and Non-factorisable Effects	21
3.4.2	Information from CP Asymmetries	26
4	Prospects for the LHCb Upgrade and Belle II Era	29
4.1	Extrapolating from Current Results	30
4.2	Exchange and Penguin Annihilation Contributions	31
4.3	Future Scenarios	32
5	Conclusions	39
	Appendix: Notation	40

1 Introduction

CP-violating effects offer important tools to search for new physics (NP) beyond the Standard Model (SM). In this endeavour, $B_q^0-\bar{B}_q^0$ mixing ($q = d, s$) is a key player. This phenomenon does not arise at the tree level in the SM and may induce interference effects between oscillation and decay processes, resulting in “mixing-induced” CP violation. The BaBar and Belle experiments at the e^+e^- B -factories and the LHCb experiment at the Large Hadron Collider (LHC) have already performed high precision measurements of the $B_d^0-\bar{B}_d^0$ and $B_s^0-\bar{B}_s^0$ mixing phases ϕ_d and ϕ_s , respectively [1, 2]. In the era of the Belle II [4] and LHCb upgrade [3], the experimental analysis will be pushed towards new frontiers of precision.

In this paper, we present an analysis of the decays $B_d^0 \rightarrow D_d^- D_d^+$ and $B_s^0 \rightarrow D_s^- D_s^+$ which are related to each other through the U -spin symmetry of strong interactions [5, 6]. With the help of this flavour symmetry, penguin effects can be included in the determination of ϕ_d and ϕ_s from the mixing-induced CP asymmetries of these decays. The theoretical precision is limited by non-factorisable U -spin-breaking effects. The impact of these contributions can be probed in a clean way by comparing branching ratio measurements of the non-leptonic decays with data from semileptonic $B_d^0 \rightarrow D_d^- \ell^+ \nu_\ell$ and $B_s^0 \rightarrow D_s^- \ell^+ \nu_\ell$ decays. The use of the latter two modes is a new element in this strategy. We also explore the role of exchange and penguin annihilation topologies, which govern the decays $B_d^0 \rightarrow D_s^- D_s^+$ and $B_s^0 \rightarrow D_d^- D_d^+$ [7]. These modes are also related to each other by the U -spin symmetry of strong interactions.

The analysis of the $B_d^0 \rightarrow D_d^- D_d^+$, $B_s^0 \rightarrow D_s^- D_s^+$ system complements the determination of ϕ_d and ϕ_s from the decays $B_d^0 \rightarrow J/\psi K_S^0$ and $B_s^0 \rightarrow J/\psi \phi$, respectively, where penguin effects have to be included as well [5, 8–17]. The dynamics of the $B \rightarrow D\bar{D}$ modes differs from those of the $B \rightarrow J/\psi X$ channels. In the latter case, the QCD penguins require a colour-singlet exchange and are suppressed by the Okubo–Zweig–Iizuka (OZI) rule [18–20], while this feature does not apply to the electroweak (EW) penguins, which are colour-allowed and hence contribute significantly to the decay amplitudes [21]. On the other hand, the QCD penguins are not OZI suppressed in the $B_d^0 \rightarrow D_d^- D_d^+$, $B_s^0 \rightarrow D_s^- D_s^+$ system, whereas the EW penguins contribute only in colour-suppressed form. The EW penguin sector offers an interesting avenue for NP to enter weak meson decays [22–25], such as in models with extra Z' bosons [26, 27], and would then lead to discrepancies in the determined values of ϕ_d and ϕ_s should the Z' bosons have CP-violating flavour-changing couplings to quarks.

The outline of this paper is as follows: in Section 2, we discuss the decay amplitude structure of the $B_d^0 \rightarrow D_d^- D_d^+$, $B_s^0 \rightarrow D_s^- D_s^+$ decays and their observables, while we turn to the picture emerging from the current data in Section 3. There, we include additional decay modes, which have dynamics similar to the $B_d^0 \rightarrow D_d^- D_d^+$, $B_s^0 \rightarrow D_s^- D_s^+$ system, to address the importance of exchange and penguin annihilation topologies, and probe non-factorisable effects by means of the differential $B_d^0 \rightarrow D_d^- \ell^+ \nu_\ell$ rate. We perform a global analysis of the penguin parameters a and θ , which allows us to extract ϕ_d and ϕ_s from measurements of CP violation in the $B_d^0 \rightarrow D_d^- D_d^+$ and $B_s^0 \rightarrow D_s^- D_s^+$ modes, respectively. The current uncertainties of these measurements are unfortunately still very large. In Section 4, we focus on the era of the Belle II and LHCb upgrade, and explore the prospects by discussing different scenarios. Finally, we summarise our conclusions in Section 5. In an appendix, we give a summary of the various parameters and observables used in our analysis.

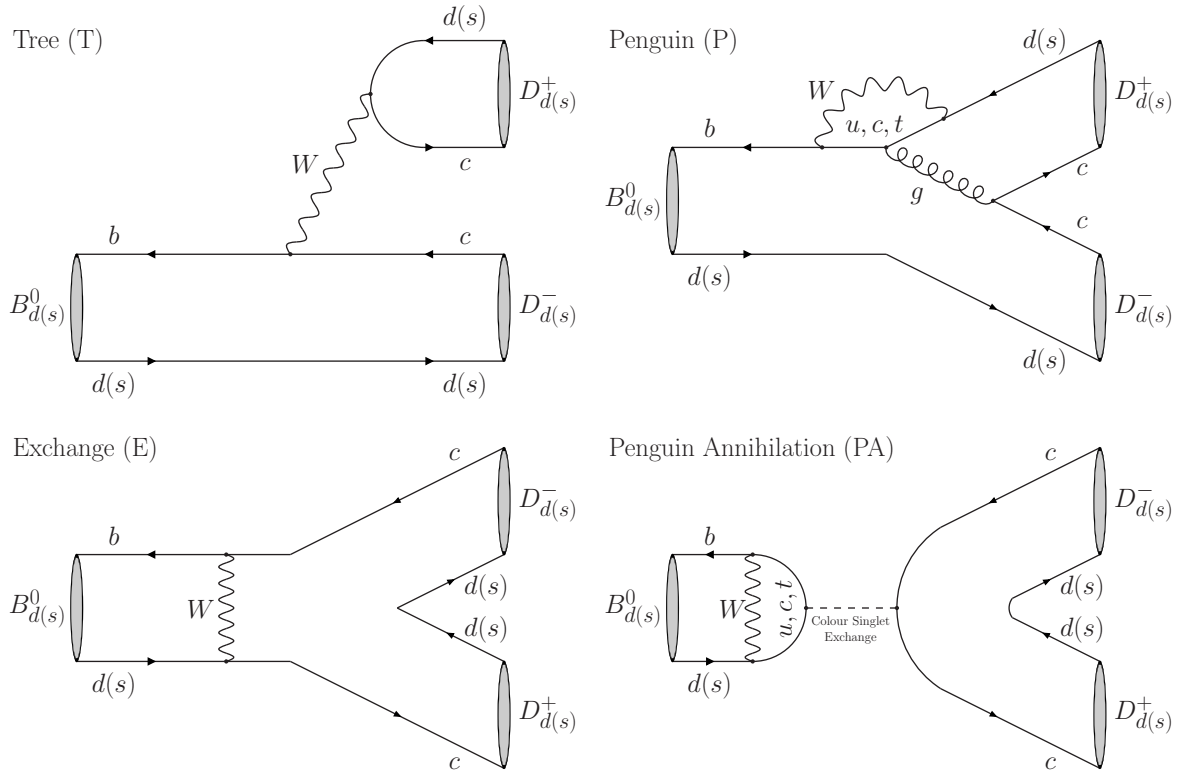


Figure 1: Illustration of topologies contributing to the $B_{d(s)}^0 \rightarrow D_{d(s)}^+ D_{d(s)}^-$ decays.

2 Decay Amplitudes and Observables

2.1 Amplitude Structure

The $B_d^0 \rightarrow D_d^- D_d^+$ mode is caused by $\bar{b} \rightarrow \bar{c} \bar{d}$ quark-level transitions, and in the SM receives contributions from the decay topologies illustrated in Fig. 1. The decay amplitude takes the following form [5]:

$$A(B_d^0 \rightarrow D_d^- D_d^+) = -\lambda \mathcal{A} [1 - ae^{i\theta} e^{i\gamma}] , \quad (1)$$

where γ serves as a CP-violating weak phase and is the usual angle of the unitarity triangle (UT) of the Cabibbo–Kobayashi–Maskawa (CKM) matrix [28, 29], while

$$\mathcal{A} \equiv \lambda^2 A [T + E + \{P^{(c)} + PA^{(c)}\} - \{P^{(t)} + PA^{(t)}\}] \quad (2)$$

and

$$ae^{i\theta} \equiv R_b \left[\frac{\{P^{(u)} + PA^{(u)}\} - \{P^{(t)} + PA^{(t)}\}}{T + E + \{P^{(c)} + PA^{(c)}\} - \{P^{(t)} + PA^{(t)}\}} \right] \quad (3)$$

are CP-conserving hadronic parameters. Here T and $P^{(q)}$ denote the strong amplitudes of the (colour-allowed) tree and penguin topologies (with internal q -quark exchanges), respectively, which can be expressed in terms of hadronic matrix elements of the corresponding low-energy effective Hamiltonian. We have also included the amplitudes describing exchange E and penguin annihilation $PA^{(q)}$ topologies, which are naively expected to play a minor role [30]. However, we find that the current data imply sizeable

contributions for $E + PA^{(c)} - PA^{(t)}$ with respect to $T + P^{(c)} - P^{(t)}$. The parameter

$$R_b \equiv \left(1 - \frac{\lambda^2}{2}\right) \frac{1}{\lambda} \left| \frac{V_{ub}}{V_{cb}} \right| = 0.390 \pm 0.031 \quad (4)$$

measures the side of the UT originating from the origin of the complex plane with the angle γ between the real axis, while $\lambda \equiv |V_{us}| = 0.22548 \pm 0.00068$ is the Wolfenstein parameter of the CKM matrix [31], and $A \equiv |V_{cb}|/\lambda^2 = 0.806 \pm 0.017$; the numerical values refer to the analysis of Ref. [32].

The U -spin partner $B_s^0 \rightarrow D_s^- D_s^+$ of the $B_d^0 \rightarrow D_d^- D_d^+$ channel originates from the $\bar{b} \rightarrow \bar{c} c \bar{s}$ quark-level processes. Its SM transition amplitude can be written as

$$A(B_s^0 \rightarrow D_s^- D_s^+) = \left(1 - \frac{\lambda^2}{2}\right) \mathcal{A}' \left[1 + \epsilon a' e^{i\theta'} e^{i\gamma}\right], \quad (5)$$

where the hadronic parameters \mathcal{A}' and $a' e^{i\theta'}$ are given by expressions which are analogous to those in Eqs. (2) and (3), respectively. The key difference in the structure of the $B_s^0 \rightarrow D_s^- D_s^+$ decay amplitude with respect to Eq. (1) is the suppression of the $a' e^{i\theta'} e^{i\gamma}$ term by the tiny CKM parameter

$$\epsilon \equiv \frac{\lambda^2}{1 - \lambda^2} = 0.0536 \pm 0.0003. \quad (6)$$

Moreover, the overall factor of λ is absent, thereby enhancing the decay rate with respect to $B_d^0 \rightarrow D_d^- D_d^+$. Therefore, sizeable penguin effects in $B_d^0 \rightarrow D_d^- D_d^+$ could be probed and subsequently used to estimate the penguin effects in $B_s^0 \rightarrow D_s^- D_s^+$, applying U -spin symmetry.

The U -spin symmetry of strong interactions implies the following relations between the hadronic parameters:

$$a e^{i\theta} = a' e^{i\theta'}, \quad (7)$$

$$\mathcal{A} = \mathcal{A}'. \quad (8)$$

It is important to emphasise that hadronic form factors and decay constants cancel within factorisation in $a e^{i\theta}$ and $a' e^{i\theta'}$, since these quantities are defined as ratios of hadronic amplitudes, as can be seen in Eq. (3). Consequently, factorisable U -spin-breaking corrections to the relation in Eq. (7) vanish [5, 6]. On the other hand, the U -spin relation in Eq. (8) is affected by $SU(3)$ -breaking effects¹ in $B_q \rightarrow D_q$ form factors and D_q decay constants ($q = d, s$). We discuss these effects in more detail later.

2.2 CP-Violating Asymmetries

Due to $B_q^0 - \bar{B}_q^0$ oscillations ($q = d, s$), an initially present B_q^0 -meson state evolves in time into a linear combination of B_q^0 and \bar{B}_q^0 states. CP violation in the $B_q^0 \rightarrow D_q^- D_q^+$ decays, which are characterised by CP-even final states, is probed through the following

¹ $SU(3)$ symmetry refers to the symmetry group interchanging u, d and s quarks. The isospin, U -spin and V -spin subgroups refer to interchanging $u \leftrightarrow d$, $d \leftrightarrow s$, and $s \leftrightarrow u$, respectively. Throughout the paper the mention of $SU(3)$ refers to the U -spin subgroup, unless specified otherwise.

time-dependent rate asymmetries [33]:

$$\begin{aligned} & \frac{|A(B_q^0(t) \rightarrow D_q^- D_q^+)|^2 - |A(\bar{B}_q^0(t) \rightarrow D_q^- D_q^+)|^2}{|A(B_q^0(t) \rightarrow D_q^- D_q^+)|^2 + |A(\bar{B}_q^0(t) \rightarrow D_q^- D_q^+)|^2} \\ &= \frac{\mathcal{A}_{\text{CP}}^{\text{dir}}(B_q \rightarrow D_q^- D_q^+) \cos(\Delta M_q t) + \mathcal{A}_{\text{CP}}^{\text{mix}}(B_q \rightarrow D_q^- D_q^+) \sin(\Delta M_q t)}{\cosh(\Delta \Gamma_q t/2) + \mathcal{A}_{\Delta\Gamma}(B_q \rightarrow D_q^- D_q^+) \sinh(\Delta \Gamma_q t/2)}, \end{aligned} \quad (9)$$

where $\Delta M_q \equiv M_{\text{H}}^{(q)} - M_{\text{L}}^{(q)}$ and $\Delta \Gamma_q \equiv \Gamma_{\text{L}}^{(q)} - \Gamma_{\text{H}}^{(q)}$ denote the mass and decay width difference between the two B_q mass eigenstates, respectively. The three CP observables are given by²

$$\mathcal{A}_{\text{CP}}^{\text{dir}}(B_q \rightarrow D_q^- D_q^+) = \frac{2b_q \sin \rho_q \sin \gamma}{1 - 2b_q \cos \rho_q \cos \gamma + b_q^2}, \quad (10)$$

$$\mathcal{A}_{\text{CP}}^{\text{mix}}(B_q \rightarrow D_q^- D_q^+) = \eta_q \left[\frac{\sin \phi_q - 2b_q \cos \rho_q \sin(\phi_q + \gamma) + b_q^2 \sin(\phi_q + 2\gamma)}{1 - 2b_q \cos \rho_q \cos \gamma + b_q^2} \right], \quad (11)$$

$$\mathcal{A}_{\Delta\Gamma}(B_q \rightarrow D_q^- D_q^+) = -\eta_q \left[\frac{\cos \phi_q - 2b_q \cos \rho_q \cos(\phi_q + \gamma) + b_q^2 \cos(\phi_q + 2\gamma)}{1 - 2b_q \cos \rho_f \cos \gamma + b_q^2} \right], \quad (12)$$

where we have to make the following replacements for the decays at hand [5]:

$$B_d^0 \rightarrow D_d^- D_d^+ : b_d e^{i\rho_d} = a e^{i\theta}, \quad B_s^0 \rightarrow D_s^- D_s^+ : b_s e^{i\rho_s} = -\epsilon a' e^{i\theta'}. \quad (13)$$

The parameter η_q denotes the CP eigenvalue of the final state and is given by +1. While the direct CP asymmetries $\mathcal{A}_{\text{CP}}^{\text{dir}}(B_q \rightarrow D_q^- D_q^+)$ are caused by interference between tree and penguin contributions, the mixing-induced CP asymmetries $\mathcal{A}_{\text{CP}}^{\text{mix}}(B_q \rightarrow D_q^- D_q^+)$ originate from interference between B_q^0 - \bar{B}_q^0 mixing and decay processes, and depend on the mixing phases ϕ_d and ϕ_s . These quantities take the general forms

$$\phi_d = 2\beta + \phi_d^{\text{NP}}, \quad \phi_s = -2\beta_s + \phi_s^{\text{NP}}, \quad (14)$$

where β is the usual angle of the UT. The SM value of ϕ_s , which is given by $-2\beta_s = -2\lambda^2 \eta$ and hence doubly Cabibbo suppressed, can be determined with high precision from SM fits of the UT [32]:

$$\phi_s^{\text{SM}} = -(2.092_{-0.069}^{+0.075})^\circ. \quad (15)$$

The CP-violating phases ϕ_q^{NP} vanish in the SM and allow us to take NP contributions to B_q^0 - \bar{B}_q^0 mixing into account.

It is useful to introduce “effective mixing phases”

$$\phi_{q, D_q^- D_q^+}^{\text{eff}} \equiv \phi_q + \Delta \phi_q^{D_q^- D_q^+} \quad (16)$$

through the following expression [12, 16]:

$$\frac{\mathcal{A}_{\text{CP}}^{\text{mix}}(B_q \rightarrow D_q^- D_q^+)}{\sqrt{1 - (\mathcal{A}_{\text{CP}}^{\text{dir}}(B_q \rightarrow D_q^- D_q^+))^2}} = \sin(\phi_{q, D_q^- D_q^+}^{\text{eff}}), \quad (17)$$

²Whenever information from both $B_q^0 \rightarrow f$ and $\bar{B}_q^0 \rightarrow f$ decays is needed to determine an observable, as is the case for CP asymmetries or untagged branching ratios, we use the notation B_d and B_s .

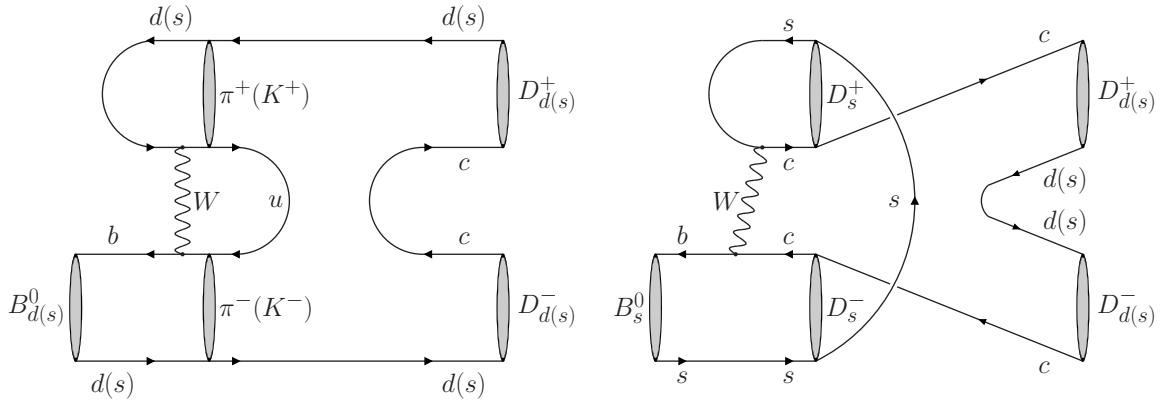


Figure 2: Illustrations of the rescattering processes in Eqs. (23) and (24).

where the hadronic “penguin phase shifts” $\Delta\phi_q^{D_q^- D_q^+}$ are characterised by

$$\tan \Delta\phi_d^{D_d^- D_d^+} = \frac{-2a \cos \theta \sin \gamma + a^2 \sin 2\gamma}{1 - 2a \cos \theta \cos \gamma + a^2 \cos 2\gamma} = -2a \cos \theta \sin \gamma - a^2 \cos 2\theta \sin 2\gamma + \mathcal{O}(a^3) \quad (18)$$

$$\tan \Delta\phi_s^{D_s^- D_s^+} = \frac{2\epsilon a' \cos \theta' \sin \gamma + \epsilon^2 a'^2 \sin 2\gamma}{1 + 2\epsilon a' \cos \theta' \cos \gamma + \epsilon^2 a'^2 \cos 2\gamma} = 2\epsilon a' \cos \theta' \sin \gamma + \mathcal{O}(\epsilon^2 a'^2). \quad (19)$$

In the limit $a = a' = 0$, we simply have

$$\mathcal{A}_{\text{CP}}^{\text{dir}}(B_d \rightarrow D_d^- D_d^+)|_{a=0} = 0, \quad \mathcal{A}_{\text{CP}}^{\text{mix}}(B_d \rightarrow D_d^- D_d^+)|_{a=0} = \sin \phi_d, \quad (20)$$

$$\mathcal{A}_{\text{CP}}^{\text{dir}}(B_s \rightarrow D_s^- D_s^+)|_{a'=0} = 0, \quad \mathcal{A}_{\text{CP}}^{\text{mix}}(B_s \rightarrow D_s^- D_s^+)|_{a'=0} = \sin \phi_s. \quad (21)$$

The penguin parameter $ae^{i\theta}$ cannot be calculated reliably within QCD. Since this quantity is governed by the ratio of a penguin amplitude to a colour-allowed tree amplitude, it is plausible to expect $a \sim 0.1$ – 0.2 . Applying the Bander–Silverman–Soni mechanism [34] and the formalism developed in Refs. [35, 36] yields the following estimate [6]:

$$ae^{i\theta}|_{\text{QCD}}^{\text{BSS}} \sim 0.08 \times e^{i205^\circ}. \quad (22)$$

In the corresponding calculation, form factors and decay constants cancel as the parameter $ae^{i\theta}$ is actually defined as a ratio of hadronic amplitudes, as we emphasised after Eq. (8). However, incalculable long-distance contributions, such as processes of the kind

$$B_d^0 \rightarrow [\pi^- \pi^+, \rho^- \pi^+, \dots] \rightarrow D_d^- D_d^+, \quad B_s^0 \rightarrow [K^- K^+, K^{*-} K^+, \dots] \rightarrow D_s^- D_s^+, \quad (23)$$

and

$$B_d^0 \rightarrow [D_d^- D_d^+, D_d^{*-} D_d^+, \dots] \rightarrow D_d^- D_d^+, \quad B_s^0 \rightarrow [D_s^- D_s^+, D_s^{*-} D_s^+, \dots] \rightarrow D_s^- D_s^+, \quad (24)$$

which can be considered as long-distance penguins with up- and charm-quark exchanges [37], respectively, as illustrated in Fig. 2, may have an impact on $ae^{i\theta}$.

In this paper, we discuss strategies to control these effects by means of experimental data. In the $B_d^0 \rightarrow D_d^- D_d^+$ case (Eq. (20)), the penguin effects have to be taken into account for the determination of ϕ_d . In the $B_s^0 \rightarrow D_s^- D_s^+$ case (Eq. (21)), the parameter a' is associated with the tiny ϵ factor and is hence doubly Cabibbo-suppressed. However, in view of the experimental precision in the LHCb upgrade era, also these effects have to be controlled.

2.3 Untagged Decay Rate Information

For the analysis of the experimental data later on, it is useful to introduce another observable, containing the untagged rate information. It is defined as [5, 6]:

$$H \equiv \frac{1}{\epsilon} \left| \frac{\mathcal{A}'}{\mathcal{A}} \right|^2 \left[\frac{m_{B_d} \Phi(m_{D_s}/m_{B_s}, m_{D_s}/m_{B_s}) \tau_{B_s}}{m_{B_s} \Phi(m_{D_d}/m_{B_d}, m_{D_d}/m_{B_d}) \tau_{B_d}} \right] \frac{\mathcal{B}(B_d \rightarrow D_d^- D_d^+)}{\mathcal{B}(B_s \rightarrow D_s^- D_s^+)_{\text{theo}}}, \quad (25)$$

where

$$\Phi(x, y) = \sqrt{[1 - (x + y)^2][1 - (x - y)^2]} \quad (26)$$

is the well-known $B \rightarrow PP$ phase-space function. Due to the sizeable lifetime difference in the B_s -meson system, $y_s \equiv \Delta\Gamma_s/2\Gamma_s = 0.0608 \pm 0.0045$ [2], a difference arises between the “theoretical” branching ratio defined through the untagged decay rate at time $t = 0$ [5] and the “experimental” branching ratio which is extracted from the time-integrated untagged rate [38]. They can be related as [39]

$$\begin{aligned} \mathcal{B}(B_s \rightarrow D_s^- D_s^+)_{\text{theo}} &= \left[\frac{1 - y_s^2}{1 + \mathcal{A}_{\Delta\Gamma}(B_s \rightarrow D_s^- D_s^+) y_s} \right] \mathcal{B}(B_s \rightarrow D_s^- D_s^+) \\ &= (1.09 \pm 0.03) \times \mathcal{B}(B_s \rightarrow D_s^- D_s^+), \end{aligned} \quad (27)$$

where the numerical estimate uses

$$\mathcal{A}_{\Delta\Gamma}(B_s \rightarrow D_s^- D_s^+) = -1.41 \pm 0.30, \quad (28)$$

extracted from the measurement of the effective $B_s^0 \rightarrow D_s^- D_s^+$ lifetime [6, 40].

The observable H takes the following form in terms of the penguin parameters [5]:

$$H = \frac{1 - 2a \cos \theta \cos \gamma + a^2}{1 + 2\epsilon a' \cos \theta' \cos \gamma + \epsilon^2 a'^2}. \quad (29)$$

Moreover, the U -spin relation in Eq. (7) implies

$$H = -\frac{1}{\epsilon} \left[\frac{\mathcal{A}_{\text{CP}}^{\text{dir}}(B_s \rightarrow D_s^- D_s^+)}{\mathcal{A}_{\text{CP}}^{\text{dir}}(B_d \rightarrow D_d^- D_d^+)} \right]. \quad (30)$$

Using Eq. (7) and keeping a and θ as free parameters, the expression in Eq. (29) results in the following lower bound [41, 42]:

$$\begin{aligned} H &\geq \frac{1 + \epsilon^2 + 2\epsilon \cos^2 \gamma - (1 + \epsilon) \sqrt{1 - 2\epsilon + \epsilon^2 + 4\epsilon \cos^2 \gamma}}{2\epsilon^2 (1 - \cos^2 \gamma)} \\ &= \sin^2 \gamma - 2\epsilon \sin^2 \gamma \cos^2 \gamma + \mathcal{O}(\epsilon^2) \xrightarrow{\gamma=73.2^\circ} 0.908. \end{aligned} \quad (31)$$

Moreover, H allows us to put a lower bound on the penguin parameter a :

$$a \geq -\left(\frac{1 + \epsilon H}{1 - \epsilon^2 H} \right) \cos \gamma + \sqrt{\left[\left(\frac{1 + \epsilon H}{1 - \epsilon^2 H} \right) \cos \gamma \right]^2 - \left(\frac{1 - H}{1 - \epsilon^2 H} \right)}. \quad (32)$$

The signs have been chosen in such a way that this expression applies to the current experimental situation discussed in Section 3.4.

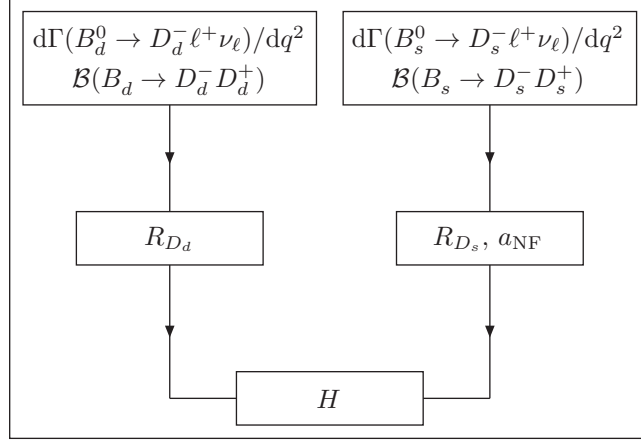


Figure 3: Flow chart illustrating the new strategy to determine H using data from semileptonic $B_q^0 \rightarrow D_q^- \ell^+ \nu_\ell$ decays.

2.4 Information from Semileptonic Decays

The experimental determination of H through Eq. (25) requires information on the amplitude ratio $|\mathcal{A}'/\mathcal{A}|$, which is affected by U -spin-breaking corrections to the relation in Eq. (8). To avoid the limitations this brings, we propose a new method to determine H using data from semileptonic $B_q^0 \rightarrow D_q^- \ell^+ \nu_\ell$ decays, which is illustrated by the flow chart in Fig. 3. To this end, we introduce the ratio

$$R_{D_q} \equiv \frac{\Gamma(B_q \rightarrow D_q^- D_q^+)_{\text{theo}}}{[\text{d}\Gamma(B_q^0 \rightarrow D_q^- \ell^+ \nu_\ell)/\text{d}q^2]_{q^2=m_{D_q}^2}} \quad (33)$$

$$= 6\pi^2 |V_{cq}|^2 f_{D_q}^2 X_{D_q} \left| a_{\text{NF}}^{(q)} \right|^2 [1 - 2b_q \cos \rho_q \cos \gamma + b_q^2], \quad (34)$$

where the parameters b_q and ρ_q are given in Eq. (13); V_{cq} is the relevant CKM matrix element, f_{D_q} denotes the D_q -meson decay constant defined through

$$\langle D_q^-(p) | \bar{q} \gamma_\mu \gamma_5 c | 0 \rangle = -i f_{D_q} p_\mu, \quad (35)$$

and the factor X_{D_q} is given by

$$X_{D_q} = \left[\frac{(m_{B_q}^2 - m_{D_q}^2)^2}{m_{B_q}^2 (m_{B_q}^2 - 4m_{D_q}^2)} \right] \left[\frac{F_0^{B_q D_q}(m_{D_q}^2)}{F_1^{B_q D_q}(m_{D_q}^2)} \right]^2, \quad (36)$$

where the form factors are defined through

$$\begin{aligned} & \langle D_q^+(k) | \bar{c} \gamma_\mu b | \bar{B}_q^0(p) \rangle \\ &= F_1^{B_q D_q}(q^2) \left[(p+k)_\mu - \left(\frac{m_{B_q}^2 - m_{D_q}^2}{q^2} \right) q_\mu \right] + F_0^{B_q D_q}(q^2) \left(\frac{m_{B_q}^2 - m_{D_q}^2}{q^2} \right) q_\mu, \end{aligned} \quad (37)$$

with $q \equiv p - k$. Ratios between non-leptonic decay rates and differential semileptonic rates as in Eq. (33) are well-known probes for testing factorisation [43–48].

The parameter $a_{\text{NF}}^{(q)}$ measures non-factorisable effects in the amplitudes defined through Eq. (2), which we may write as

$$\mathcal{A}_q \equiv \lambda^2 A T_{\text{fact}}^{(q)} a_{\text{NF}}^{(q)}, \quad (38)$$

where

$$T_{\text{fact}}^{(q)} = -i \frac{G_{\text{F}}}{\sqrt{2}} f_{D_q} \left(m_{B_q}^2 - m_{D_q}^2 \right) F_0^{B_q D_q}(m_{D_q}^2) \quad (39)$$

is the amplitude of the colour-allowed tree topology in factorisation, with G_{F} denoting Fermis constant. In naive factorisation, $a_{\text{NF}}^{(q)} = a_1$, where a_1 represents the appropriate combination of Wilson coefficient functions of the current-current operators³. We have $\mathcal{A} \equiv \mathcal{A}_d$ and $\mathcal{A}' \equiv \mathcal{A}_s$, and shall suppress the label q in the following discussion for simplicity. Introducing the abbreviations

$$P^{(ct)} \equiv P^{(c)} - P^{(t)}, \quad PA^{(ct)} \equiv PA^{(c)} - PA^{(t)}, \quad (40)$$

we obtain

$$a_{\text{NF}} = (1 + r_P)(1 + x) a_{\text{NF}}^T, \quad (41)$$

where

$$r_P \equiv \frac{P^{(ct)}}{T} \quad (42)$$

measures the importance of the penguin topologies with respect to the colour-allowed tree amplitude. On the other hand,

$$x \equiv |x| e^{i\sigma} \equiv \frac{E + PA^{(ct)}}{T + P^{(ct)}} \quad (43)$$

probes the importance of the exchange and penguin annihilation topologies. We will return to x in Subsection 3.3.2, where we determine $|x|$ and the CP-conserving strong phase σ from experimental data. The parameter a_{NF}^T describes the non-factorisable corrections to the “tree” diagram (Eq. (39)), i.e. we have

$$T = T_{\text{fact}} a_{\text{NF}}^T \equiv T_{\text{fact}} [1 + \Delta_{\text{NF}}^T] \quad (44)$$

with $\Delta_{\text{NF}}^T = 0$ for exact factorisation.

Finally, the observable H can be expressed as follows:

$$H = \left| \frac{V_{cs}}{V_{cd}} \right|^2 \left[\frac{R_{D_d}}{R_{D_s}} \right] \left[\frac{f_{D_s}}{f_{D_d}} \right]^2 \left[\frac{X_{D_s}}{X_{D_d}} \right] \left| \frac{a_{\text{NF}}^{(s)}}{a_{\text{NF}}^{(d)}} \right|^2. \quad (45)$$

In comparison with Eq. (25), the advantage is that the theoretical precision is now only limited by *non-factorisable* U -spin-breaking effects. Moreover, as the R_{D_q} are ratios of B_q rates, the dependence on the ratio of fragmentation functions f_s/f_d , which is needed for normalisation purposes [50], drops out in this expression.

It is instructive to have a closer look at the non-factorisable U -spin-breaking effects entering Eq. (45), although we will constrain them through experimental data. We obtain the following expression:

$$\left| \frac{a_{\text{NF}}^{(s)}}{a_{\text{NF}}^{(d)}} \right| \equiv \left| \frac{1 + \Delta_{\text{NF}}^{(s)}}{1 + \Delta_{\text{NF}}^{(d)}} \right| = \left| \frac{1 + r_P^{(s)}}{1 + r_P^{(d)}} \right| \left| \frac{1 + x^{(s)}}{1 + x^{(d)}} \right| \left| \frac{1 + \Delta_{\text{NF}}^{T(s)}}{1 + \Delta_{\text{NF}}^{T(d)}} \right|. \quad (46)$$

³For a detailed discussion, see Ref. [49].

Using heavy-meson chiral perturbation theory and the $1/N_C$ expansion, non-factorisable $SU(3)$ -breaking corrections to the colour-allowed tree amplitudes of $B_q^0 \rightarrow D_q \bar{D}_p$ decays were found at the level of a few percent in Ref. [51], suggesting small corrections from the last factor. The U -spin relation between the $B_s^0 \rightarrow D_s^- D_s^+$ and $B_d^0 \rightarrow D_d^- D_d^+$ decays is reflected by the one-to-one correspondence of the $r_P^{(q)}$ and $x^{(q)}$ terms. These contributions enter Eq. (46) only in ratios of terms with structures $1 + \Lambda^{(q)}$, where we expect the $\Lambda^{(q)}$ to be at most $\mathcal{O}(0.2)$. Assuming $SU(3)$ -breaking at the 30% level for the $\Lambda^{(q)}$ terms yields a correction of only $\mathcal{O}(5\%)$ for the ratios, i.e. a robust situation.

Let us now exploit experimental data to probe these effects. Using the ratio R_{D_s} , we may actually determine $|a_{\text{NF}}^{(s)}|$ with the help of the relation

$$|a_{\text{NF}}^{(s)}| \equiv 1 + \Delta_{\text{NF}}^{(s)} = [1 - \epsilon a' \cos \theta' \cos \gamma + \mathcal{O}(\epsilon^2 a'^2)] \sqrt{\frac{R_{D_s}}{6\pi^2 |V_{cs}|^2 f_{D_s}^2 X_{D_s}}}, \quad (47)$$

where $\Delta_{\text{NF}}^{(s)}$ is now — by definition — a real parameter and the corrections due to the $\epsilon a'$ term are at most at the level of a few percent. Assuming

$$\Delta_{\text{NF}}^{(d)} = \Delta_{\text{NF}}^{(s)} [1 - \xi_{SU(3)}] \quad (48)$$

with the $SU(3)$ -breaking parameter $\xi_{SU(3)} \propto m_s/\Lambda_{\text{QCD}}$, we obtain

$$\left| \frac{a_{\text{NF}}^{(s)}}{a_{\text{NF}}^{(d)}} \right| = \frac{1 + \Delta_{\text{NF}}^{(s)}}{1 + \Delta_{\text{NF}}^{(s)} [1 - \xi_{SU(3)}]} = 1 + \Delta_{\text{NF}}^{(s)} \xi_{SU(3)} + \mathcal{O}(\Delta_{\text{NF}}^{(s)2}). \quad (49)$$

Consequently, the information for the semileptonic differential rate allows us to quantify the non-factorisable U -spin-breaking corrections to the determination of H (Eq. (45)).

Let us now return to discuss the remaining quantities entering Eq. (45). The D_q -meson decay constants ($q = d, s$) can be extracted from leptonic decays:

$$\Gamma(D_q^+ \rightarrow \mu^+ \nu_\mu) = \frac{G_F^2}{8\pi} m_{D_q} m_\mu^2 \left[1 - \left(\frac{m_\mu}{m_{D_q}} \right)^2 \right] |V_{cq}|^2 f_{D_q}^2. \quad (50)$$

The current experimental status has been summarised in Ref. [52]:

$$f_{D_s} = (257.5 \pm 4.6) \text{ MeV}, \quad f_{D_d} = (204.6 \pm 5.0) \text{ MeV}, \quad f_{D_s}/f_{D_d} = 1.258 \pm 0.038. \quad (51)$$

A detailed overview of the status of lattice QCD calculations has been given by the FLAG Working Group in Ref. [53].

In the infinite quark-mass limit, the following consistency relation arises [54]:

$$\frac{F_0^{B_q D_q}(q^2)}{F_1^{B_q D_q}(q^2)} = 1 - \frac{q^2}{(m_{B_q} + m_{D_q})^2}. \quad (52)$$

For a discussion on QCD and Λ_{QCD}/m_Q corrections to this relation we refer the reader to Refs. [54–56]. There has recently been impressive progress in the calculation of hadronic form factors within lattice QCD, where now the first unquenched calculations of the $\bar{B} \rightarrow \bar{D} \ell \bar{\nu}_\ell$ form factors at nonzero recoil are available [57, 58]. Using the results of Ref. [58], we obtain

$$\frac{F_0^{B_q D_q}(m_{D_s}^2)}{F_1^{B_q D_q}(m_{D_s}^2)} = 0.917 \pm 0.079, \quad (53)$$

while the expression in Eq. (52) gives 0.924, thereby indicating small corrections. In the numerical analysis in this paper, we will use the result in Eq. (53).

Experimental data for the semileptonic decay $B_s^0 \rightarrow D_s^- \ell^+ \nu_\ell$ is not yet available. Although it is experimentally challenging to disentangle the semileptonic $B_s^0 \rightarrow D_s^- \ell^+ \nu_\ell$ and $B_s^0 \rightarrow D_s^{*-} \ell^+ \nu_\ell$ decays, it might be feasible to distinguish them due to the shifted invariant mass spectrum of the $D_s^+ \mu^-$ combinations, and the difference in the missing reconstructed mass, which is correlated to the “corrected mass” as illustrated in Ref. [59]. Combined with a fit to the angular distributions, this gives information on the different form factors. We encourage to add this channel to the experimental agenda of the LHCb and Belle II experiments and perform detailed studies for the upgrade era. On the other hand, the differential rate of the $B_d^0 \rightarrow D_d^- \ell^+ \nu_\ell$ mode has already been measured and will actually be used in the next section to estimate the non-factorisable effects in B_d^0 decays.

The lack of experimental data on semileptonic B_s^0 decays can be circumvented by studying the ratio of other B_d^0 and B_s^0 decays, discussed in the next Section, and applying $SU(3)$ flavour symmetry. The $SU(3)$ -breaking non-factorisable effects in the ratio of B_d^0 and B_s^0 decays are estimated from the deviation from factorisation in B_d^0 decays.

3 Picture Emerging from the Current Data

3.1 Overview

The main objective of this analysis is the determination of the $B_q^0-\bar{B}_q^0$ mixing phases ϕ_d and ϕ_s from the $B_d^0 \rightarrow D_d^- D_d^+$ and $B_s^0 \rightarrow D_s^- D_s^+$ channels, respectively. High precision determinations of these phases require us to control not only the contributions from penguin topologies, but also the impact of additional decay topologies and non-factorisable effects. The latter two aspects cannot be quantified using information from the $B_d^0 \rightarrow D_d^- D_d^+$ and $B_s^0 \rightarrow D_s^- D_s^+$ decays alone. Additional $B \rightarrow D\bar{D}$ decays with similar dynamics to the $B_d^0 \rightarrow D_d^- D_d^+$, $B_s^0 \rightarrow D_s^- D_s^+$ system therefore need to be studied. An overview of the different decay modes discussed in this section and their applications is given in Table 1.

3.2 Preliminaries

The direct and mixing-induced CP asymmetries of the $B_d^0 \rightarrow D_d^- D_d^+$ decay and the H observable, when using the U -spin relation in Eq. (7), depend on the four parameters a , θ , ϕ_d and γ . In 1999, when this decay was originally suggested by one of us, the determination of the UT angle γ was the main goal. The proposed strategy therefore assumed input on ϕ_d , determined from $B_d^0 \rightarrow J/\psi K_S^0$ and complemented with $B_s^0 \rightarrow J/\psi K_S^0$ [16], to determine a , θ and γ from $\mathcal{A}_{\text{CP}}^{\text{dir}}(B_d \rightarrow D_d^- D_d^+)$, $\mathcal{A}_{\text{CP}}^{\text{mix}}(B_d \rightarrow D_d^- D_d^+)$ and H [5]. However, at present it is possible to extract γ in a powerful way through pure $B \rightarrow D^{(*)} K^{(*)}$ tree decays. Using current data for these channels, the CKMfitter and UTfit collaborations have obtained the following averages:

$$\gamma = (73.2_{-7.0}^{+6.3})^\circ \quad (\text{CKMfitter [32]}), \quad \gamma = (68.3 \pm 7.5)^\circ \quad (\text{UTfit [60]}). \quad (54)$$

For the numerical analysis in this paper, we shall use the CKMfitter result. By the time of the Belle II and LHCb upgrade era, much more precise measurements of γ from pure tree

Decay	\mathcal{A}	Topologies					Used for:
		T	P	E	PA	A	
$B_d^0 \rightarrow D_d^- D_d^+$	\mathcal{A}	x	x	x	x		determination of a and θ (and ϕ_d)
$B_d^0 \rightarrow D_d^- D_s^+$	$\tilde{\mathcal{A}}'$	x	x				non-factorisable effect \tilde{a}'_{NF}
$B_d^0 \rightarrow D_s^- D_s^+$	\mathcal{A}_{EPA}			x	x		quantify $E + PA$ contribution \tilde{x}
$B_s^0 \rightarrow D_s^- D_s^+$	\mathcal{A}'	x	x	x	x		physics goal ϕ_s
$B_s^0 \rightarrow D_s^- D_d^+$	$\tilde{\mathcal{A}}$	x	x				$SU(3)$ breaking non-fact. $\tilde{a}_{\text{NF}}/\tilde{a}'_{\text{NF}}$
$B_s^0 \rightarrow D_d^- D_d^+$	\mathcal{A}'_{EPA}			x	x		quantify $E + PA$ contribution \tilde{x}'
$B^+ \rightarrow \bar{D}^0 D_d^+$	$\tilde{\mathcal{A}}_c$	x	x			x	quantify A contribution $r_A \dots$
$B^+ \rightarrow \bar{D}^0 D_s^+$	$\tilde{\mathcal{A}}'_c$	x	x			x	\dots and consistency of $a_{\text{NF},c}/a'_{\text{NF},c}$

Table 1: Overview of the various topologies contributing to the $B \rightarrow D\bar{D}$ decays. The naming convention is indicated in the second column.

decays will be available (see Section 4). Using γ as an input, we may instead determine ϕ_d and the penguin parameters from H and the CP asymmetries of $B_d^0 \rightarrow D_d^- D_d^+$ [6]. The penguin parameters thus determined allow us to take their effects into account in the determination of ϕ_s from the mixing-induced CP asymmetry $\mathcal{A}_{\text{CP}}^{\text{mix}}(B_s \rightarrow D_s^- D_s^+)$.

3.3 Comparing $B \rightarrow D\bar{D}$ Branching Fractions

To quantify the contributions from additional decay topologies and the impact of non-factorisable effects in the $B_d^0 \rightarrow D_d^- D_d^+$, $B_s^0 \rightarrow D_s^- D_s^+$ system, we need to extend the decay basis to modes with dynamics similar to the $B_d^0 \rightarrow D_d^- D_d^+$ and $B_s^0 \rightarrow D_s^- D_s^+$ decays. If we replace the spectator quarks correspondingly, we obtain the $B_s^0 \rightarrow D_s^- D_d^+$ and $B_d^0 \rightarrow D_d^- D_s^+$ channels. These decays are again related to each other through the U -spin symmetry. However, the exchange and penguin annihilation topologies do not have counterparts in $B_s^0 \rightarrow D_s^- D_d^+$ and $B_d^0 \rightarrow D_d^- D_s^+$, which are characterised by the following decay amplitudes:

$$A(B_s^0 \rightarrow D_s^- D_d^+) = -\lambda \tilde{\mathcal{A}} \left[1 - \tilde{a} e^{i\tilde{\theta}} e^{i\gamma} \right] \quad (55)$$

$$A(B_d^0 \rightarrow D_d^- D_s^+) = \left(1 - \frac{\lambda^2}{2} \right) \tilde{\mathcal{A}}' \left[1 + \epsilon \tilde{a}' e^{i\tilde{\theta}'} e^{i\gamma} \right], \quad (56)$$

where

$$\tilde{\mathcal{A}} \equiv \lambda^2 A \left[\tilde{T} + \tilde{P}^{(c)} - \tilde{P}^{(t)} \right] \quad (57)$$

$$\tilde{a} e^{i\tilde{\theta}} \equiv R_b \left[\frac{\tilde{P}^{(u)} - \tilde{P}^{(t)}}{\tilde{T} + \tilde{P}^{(c)} - \tilde{P}^{(t)}} \right]; \quad (58)$$

$\tilde{\mathcal{A}}'$ and $\tilde{a}' e^{i\tilde{\theta}'}$ take analogous expressions. If we use the U -spin flavour symmetry, we obtain the following relations:

$$\tilde{a} e^{i\tilde{\theta}} = \tilde{a}' e^{i\tilde{\theta}'}, \quad \tilde{\mathcal{A}} = \tilde{\mathcal{A}}'. \quad (59)$$

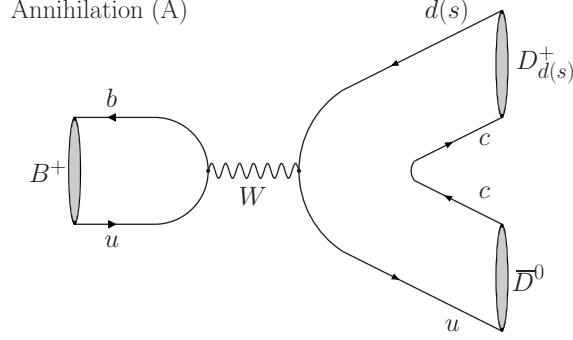


Figure 4: Illustration of the annihilation topology contributing to $B^+ \rightarrow \bar{D}^0 D_{d(s)}^+$.

Moreover, there are the charged decays $B^+ \rightarrow \bar{D}^0 D_d^+$ and $B^+ \rightarrow \bar{D}^0 D_s^+$, which are again related to each other through the U -spin symmetry. These modes also do not receive contributions from exchange and penguin annihilation topologies. However, there are additional contributions from annihilation topologies, as illustrated in Fig. 4, which enter with the same CKM factor as the penguin contributions with up-quark exchanges.

3.3.1 Probing Annihilation Topologies with Charged B decays

The decay amplitudes take the following forms:

$$A\left(B^+ \rightarrow \bar{D}^0 D_d^+\right) = -\lambda \tilde{\mathcal{A}}_c \left[1 - \tilde{a}_c e^{i\tilde{\theta}_c} e^{i\gamma}\right] \quad (60)$$

$$A\left(B^+ \rightarrow \bar{D}^0 D_s^+\right) = \left(1 - \frac{\lambda^2}{2}\right) \tilde{\mathcal{A}}_c' \left[1 + \epsilon \tilde{a}'_c e^{i\tilde{\theta}'_c} e^{i\gamma}\right], \quad (61)$$

where

$$\tilde{\mathcal{A}}_c \equiv \lambda^2 A \left[\tilde{T}_c + \tilde{P}_c^{(c)} - \tilde{P}_c^{(t)}\right] \quad (62)$$

$$\tilde{a}_c e^{i\tilde{\theta}_c} \equiv R_b \left[\frac{\tilde{P}_c^{(u)} - \tilde{P}_c^{(t)} + \tilde{\mathcal{A}}_c}{\tilde{T}_c + \tilde{P}_c^{(c)} - \tilde{P}_c^{(t)}}\right] \quad (63)$$

with $\tilde{\mathcal{A}}_c$ denoting the annihilation amplitude; the expressions for the primed amplitudes are analogous. The penguin parameter satisfies

$$\tilde{a}_c e^{i\tilde{\theta}_c} = \tilde{a} e^{i\tilde{\theta}} [1 + r_A] \quad (64)$$

with

$$r_A \equiv \frac{\tilde{\mathcal{A}}_c}{\tilde{P}_c^{(u)} - \tilde{P}_c^{(t)}}. \quad (65)$$

It is useful to introduce the following ratios:

$$\begin{aligned} & \Xi(B_s^- \rightarrow D_s^- D_d^+, B^\pm \rightarrow D_u D_d^\pm) \\ & \equiv \left[\frac{m_{B_s}}{m_{B^\pm}} \frac{\Phi(m_{D_u}/m_{B^\pm}, m_{D_d}/m_{B^\pm}) \tau_{B^\pm}}{\Phi(m_{D_s}/m_{B_s}, m_{D_d}/m_{B_s}) \tau_{B_s}}\right] \left[\frac{\mathcal{B}(B_s^- \rightarrow D_s^- D_d^+)_{\text{theo}}}{\mathcal{B}(B^\pm \rightarrow D_u D_d^\pm)}\right], \end{aligned} \quad (66)$$

$$\begin{aligned} & \Xi(B_d \rightarrow D_d^- D_s^+, B^\pm \rightarrow D_u D_s^\pm) \\ & \equiv \left[\frac{m_{B_d} \Phi(m_{D_u}/m_{B^\pm}, m_{D_s}/m_{B^\pm}) \tau_{B^\pm}}{m_{B^\pm} \Phi(m_{D_d}/m_{B_d}, m_{D_s}/m_{B_d}) \tau_{B_d}} \right] \left[\frac{\mathcal{B}(B_d \rightarrow D_d^- D_s^+)}{\mathcal{B}(B^\pm \rightarrow D_u D_s^\pm)} \right]. \end{aligned} \quad (67)$$

Using the expressions for the decay amplitudes given above yields

$$\Xi(B_s \rightarrow D_s^- D_d^+, B^\pm \rightarrow D_u D_d^\pm) = \left| \frac{\tilde{\mathcal{A}}}{\tilde{\mathcal{A}}_c} \right|^2 \left[\frac{1 - 2\tilde{a} \cos \tilde{\theta} \cos \gamma + \tilde{a}^2}{1 - 2\tilde{a}_c \cos \tilde{\theta}_c \cos \gamma + \tilde{a}_c^2} \right], \quad (68)$$

$$\Xi(B_d \rightarrow D_d^- D_s^+, B^\pm \rightarrow D_u D_s^\pm) = \left| \frac{\tilde{\mathcal{A}}'}{\tilde{\mathcal{A}}'_c} \right|^2 \left[\frac{1 + 2\epsilon \tilde{a}' \cos \tilde{\theta}' \cos \gamma + \epsilon^2 \tilde{a}'^2}{1 + 2\epsilon \tilde{a}'_c \cos \tilde{\theta}'_c \cos \gamma + \epsilon^2 \tilde{a}'_c^2} \right]. \quad (69)$$

If we apply the $SU(3)$ flavour symmetry (actually the V -spin subgroup), we obtain

$$\tilde{\mathcal{A}}_c = \tilde{\mathcal{A}}, \quad (70)$$

while the isospin symmetry of strong interactions implies

$$\tilde{\mathcal{A}}'_c = \tilde{\mathcal{A}}'. \quad (71)$$

If we neglect the annihilation contribution in Eq. (64) and assume the same penguin contributions in Eq. (68), i.e. $\tilde{a} = \tilde{a}_c$, we obtain

$$\Xi(B_s \rightarrow D_s^- D_d^+, B^\pm \rightarrow D_u D_d^\pm) \approx \left| \frac{\tilde{\mathcal{A}}}{\tilde{\mathcal{A}}_c} \right|^2 \xrightarrow{V\text{-spin}} 1. \quad (72)$$

A deviation from unity of this ratio would therefore imply either the presence of non-zero annihilation contributions or large $SU(3)$ -breaking effects through Eq. (70). In the case of (69), the penguin parameters are suppressed by the tiny ϵ factor and hence play a negligible role. Consequently, the ratio

$$\Xi(B_d \rightarrow D_d^- D_s^+, B^\pm \rightarrow D_u D_s^\pm) = \left| \frac{\tilde{\mathcal{A}}'}{\tilde{\mathcal{A}}'_c} \right|^2 \xrightarrow{\text{Isospin}} 1 \quad (73)$$

essentially relies on the strong isospin symmetry. The current experimental results compiled by the Particle Data Group (PDG) read as follows [1]:

$$\mathcal{B}(B_s \rightarrow D_s^- D_d^+) = (3.6 \pm 0.8) \times 10^{-4}, \quad (74)$$

$$\mathcal{B}(B_d \rightarrow D_d^- D_s^+) = (7.2 \pm 0.8) \times 10^{-3}, \quad (75)$$

$$\mathcal{B}(B^\pm \rightarrow D_u D_d^\pm) = (3.8 \pm 0.4) \times 10^{-4}, \quad (76)$$

$$\mathcal{B}(B^\pm \rightarrow D_u D_s^\pm) = (9.0 \pm 0.9) \times 10^{-3}, \quad (77)$$

and correspond to⁴

$$\Xi(B_s \rightarrow D_s^- D_d^+, B^\pm \rightarrow D_u D_d^\pm) = 1.08 \pm 0.27, \quad (78)$$

$$\Xi(B_d \rightarrow D_d^- D_s^+, B^\pm \rightarrow D_u D_s^\pm) = 0.89 \pm 0.13. \quad (79)$$

⁴Since $B_s^0 \rightarrow D_s^- D_d^+$ is a flavour-specific final state, we simply have $\mathcal{A}_{\Delta\Gamma}(B_s \rightarrow D_s^- D_d^+) = 0$ for the conversion of the time-integrated branching fraction into the theoretical branching ratio.

For the last decay combination, we may also employ the direct measurement of the ratio of the relevant branching fractions [61], which is given by

$$\frac{\mathcal{B}(B^\pm \rightarrow D_u D_s^\pm)}{\mathcal{B}(B_d \rightarrow D_d^- D_s^+)} = 1.22 \pm 0.02 \pm 0.07. \quad (80)$$

This leads to

$$\Xi(B_d \rightarrow D_d^- D_s^+, B^\pm \rightarrow D_u D_s^\pm) = 0.878 \pm 0.050, \quad (81)$$

which has a significantly smaller uncertainty with respect to Eq. (79) thanks to a cancellation of uncertainties in the directly measured ratio of branching fractions. We note the deviation from one at the 2.4σ level, which is unexpected.

3.3.2 Probing Exchange and Penguin Annihilation Topologies

The current PDG results for the CP-averaged branching ratios of the $B_d^0 \rightarrow D_d^- D_d^+$ and $B_s^0 \rightarrow D_s^- D_s^+$ decays are given as follows [1]:

$$\mathcal{B}(B_d \rightarrow D_d^- D_d^+) = (2.11 \pm 0.18) \times 10^{-4}, \quad (82)$$

$$\mathcal{B}(B_s \rightarrow D_s^- D_s^+) = (4.4 \pm 0.5) \times 10^{-3}. \quad (83)$$

In comparison with (75) and (77), the branching ratio in (83) is surprisingly small. A similar pattern — although not as pronounced in view of the larger uncertainties — is observed if we compare (82) with (74) and (76). As the $B_d^0 \rightarrow D_d^- D_d^+$ and $B_s^0 \rightarrow D_s^- D_s^+$ decays receive contributions from exchange and penguin annihilation topologies, which have no counterparts in the $B_s^0 \rightarrow D_s^- D_d^+$, $B^+ \rightarrow \bar{D}^0 D_d^+$ and $B_d^0 \rightarrow D_d^- D_s^+$, $B^+ \rightarrow \bar{D}^0 D_s^+$ modes, respectively (see Table 1), it is possible that the puzzling pattern of the data is actually due to the presence of these exchange and penguin annihilation contributions.

Let us first have a closer look at the ratio of the amplitudes of the $B_s^0 \rightarrow D_s^- D_s^+$ and $B_d^0 \rightarrow D_d^- D_d^+$ channels:

$$\frac{A(B_s^0 \rightarrow D_s^- D_s^+)}{A(B_d^0 \rightarrow D_d^- D_d^+)} = \left(\frac{\mathcal{A}'}{\tilde{\mathcal{A}}'} \right) \left[\frac{1 + \epsilon a' e^{i\theta'} e^{i\gamma}}{1 + \epsilon \tilde{a}' e^{i\tilde{\theta}'} e^{i\gamma}} \right] = \left[\frac{T' + P^{(ct)'}}{\tilde{T}' + \tilde{P}^{(ct)'}} + \tilde{x}' \right] \left[\frac{1 + \epsilon a' e^{i\theta'} e^{i\gamma}}{1 + \epsilon \tilde{a}' e^{i\tilde{\theta}'} e^{i\gamma}} \right], \quad (84)$$

where

$$\tilde{x}' \equiv |\tilde{x}'| e^{i\tilde{\alpha}'} \equiv \frac{E' + PA^{(ct)'}}{\tilde{T}' + \tilde{P}^{(ct)'}} \quad (85)$$

measures, in analogy to the parameter x introduced in Eq. (43), the importance of the exchange and penguin annihilation topologies with respect to the dominant tree topology; we use abbreviations as in Eq. (40). If we neglect the terms with the penguin parameters, which enter with the tiny ϵ , and introduce the $SU(3)$ -breaking parameter

$$\varrho' \equiv |\varrho'| e^{i\omega'} \equiv \frac{T' + P^{(ct)'}}{\tilde{T}' + \tilde{P}^{(ct)'}} = \left[\frac{T'}{\tilde{T}'} \right] \left[\frac{1 + P^{(ct)'}/T'}{1 + \tilde{P}^{(ct)'}/\tilde{T}'} \right], \quad (86)$$

we obtain the relation

$$\frac{A(B_s^0 \rightarrow D_s^- D_s^+)}{A(B_d^0 \rightarrow D_d^- D_d^+)} = \varrho' + \tilde{x}'. \quad (87)$$

The parameter ϱ' is only affected by $SU(3)$ -breaking effects entering at the spectator-quark level. Applying factorisation, where $P^{(ct)'} / T' = \tilde{P}^{(ct)'} / \tilde{T}'$ (see the comment after Eq. (22)), we obtain

$$\varrho'_{\text{fact}} = \left[\frac{m_{B_s}^2 - m_{D_s}^2}{m_{B_d}^2 - m_{D_d}^2} \right] \left[\frac{F_0^{B_s D_s}(m_{D_s}^2)}{F_0^{B_d D_d}(m_{D_s}^2)} \right] \quad (88)$$

$$= \left[\frac{m_{B_s} - m_{D_s}}{m_{B_d} - m_{D_d}} \right] \sqrt{\frac{m_{B_s} m_{D_s}}{m_{B_d} m_{D_d}}} \left[\frac{1 + w_s(m_{D_s}^2)}{1 + w_d(m_{D_s}^2)} \right] \left[\frac{\xi_s(w_s(m_{D_s}^2))}{\xi_d(w_d(m_{D_s}^2))} \right]. \quad (89)$$

Here we have taken into account the restrictions following for the corresponding $B_q \rightarrow D_q$ form factor from the heavy-quark effective theory [46]:

$$F_0^{B_q D_q}(q^2) = \left[\frac{m_{B_q} + m_{D_q}}{2\sqrt{m_{B_q} m_{D_q}}} \right] \left[1 - \frac{q^2}{(m_{B_q} + m_{D_q})^2} \right] \xi_q(w_q(q^2)), \quad (90)$$

where $\xi_q(w_q(q^2))$ is the Isgur–Wise function with

$$w_q(q^2) = \frac{m_{B_q}^2 + m_{D_q}^2 - q^2}{2m_{B_q} m_{D_q}}. \quad (91)$$

Studies of the light-quark dependence of the Isgur–Wise function were performed within heavy-meson chiral perturbation theory, indicating an enhancement of ξ_s/ξ_d at the level of 5% [62]. Applying the same formalism to f_{D_s}/f_{D_d} leads to estimates for the value of this ratio of about 1.2 [63], which are in agreement with the experimental results in Eq. (51).

Since 1992, when these calculations were pioneered, there has been a lot of progress in lattice QCD (for an overview of the state-of-the-art analyses, see Ref. [64]). The most recent result for the $SU(3)$ -breaking effects in the form factors reads as follows [65]:

$$\left[\frac{F_0^{B_s D_s}(m_\pi^2)}{F_0^{B_d D_d}(m_\pi^2)} \right] = 1.054 \pm 0.047 \pm 0.017, \quad (92)$$

which is in excellent agreement with the picture from heavy-meson chiral perturbation theory. Using this result as an input yields

$$\varrho'_{\text{fact}} = 1.078 \pm 0.051. \quad (93)$$

The error quantifies only the uncertainties related to the form factors. We cannot quantify the non-factorisable effects. However, as they enter only at the level of different spectator quarks and as already the leading $SU(3)$ -breaking effects are small, we expect a minor impact.

The ratio⁵

$$\begin{aligned} & \Xi(B_s \rightarrow D_s^- D_s^+, B_d \rightarrow D_d^- D_s^+) \\ & \equiv \left[\frac{m_{B_s} \Phi(m_{D_d}/m_{B_d}, m_{D_s}/m_{B_d}) \tau_{B_d}}{m_{B_d} \Phi(m_{D_s}/m_{B_s}, m_{D_s}/m_{B_s}) \tau_{B_s}} \right] \left[\frac{\mathcal{B}(B_s \rightarrow D_s^- D_s^+)_{\text{theo}}}{\mathcal{B}(B_d \rightarrow D_d^- D_s^+)} \right] = 0.647 \pm 0.049 \quad (94) \end{aligned}$$

⁵In view of the large uncertainty of Eq. (28), we use $\mathcal{A}_{\Delta\Gamma}(B_s \rightarrow D_s^- D_s^+) = -\cos\phi_s^{\text{SM}}$ for the conversion of the untagged experimental $B_s^0 \rightarrow D_s^- D_s^+$ branching ratio into its theoretical counterpart.

then takes the following form:

$$\Xi(B_s \rightarrow D_s^- D_s^+, B_d \rightarrow D_d^- D_d^+) = |\varrho'|^2 + 2|\varrho'| |\tilde{x}'| \cos(\omega' - \tilde{\sigma}') + |\tilde{x}'|^2, \quad (95)$$

thereby fixing a circle for \tilde{x}' in the complex plane. The numerical value in Eq. (94) refers to a direct measurement of the corresponding ratio of branching ratios [61].

For the other decay combination, we obtain

$$\frac{A(B_d^0 \rightarrow D_d^- D_d^+)}{A(B_s^0 \rightarrow D_s^- D_d^+)} = \left(\frac{\mathcal{A}}{\tilde{\mathcal{A}}} \right) \left[\frac{1 - ae^{i\theta} e^{i\gamma}}{1 - \tilde{a}e^{i\tilde{\theta}} e^{i\gamma}} \right] = \left[\frac{T + P^{(ct)}}{\tilde{T} + \tilde{P}^{(ct)}} + \tilde{x} \right] \left[\frac{1 - ae^{i\theta} e^{i\gamma}}{1 - \tilde{a}e^{i\tilde{\theta}} e^{i\gamma}} \right], \quad (96)$$

with

$$\tilde{x} \equiv |\tilde{x}| e^{i\tilde{\sigma}} \equiv \frac{E + PA^{(ct)}}{\tilde{T} + \tilde{P}^{(ct)}}. \quad (97)$$

In analogy to Eq. (86), we introduce a parameter

$$\varrho \equiv |\varrho| e^{i\omega} \equiv \frac{T + P^{(ct)}}{\tilde{T} + \tilde{P}^{(ct)}} = \left[\frac{T}{\tilde{T}} \right] \left[\frac{1 + P^{(ct)}/T}{1 + \tilde{P}^{(ct)}/\tilde{T}} \right], \quad (98)$$

which is given in factorisation by

$$\varrho_{\text{fact}} = \left[\frac{m_{B_d}^2 - m_{D_d}^2}{m_{B_s}^2 - m_{D_s}^2} \right] \left[\frac{F_0^{B_d D_d}(m_{D_d}^2)}{F_0^{B_s D_s}(m_{D_d}^2)} \right] = \frac{1}{\varrho'_{\text{fact}}} = 0.928 \pm 0.044, \quad (99)$$

neglecting the tiny difference between the form-factor ratios for $q^2 = m_{D_d}^2$ and $m_{D_s}^2$. As in Eq. (93), the error quantifies only the form factor uncertainties.

The penguin parameters do not enter Eq. (96) with the tiny ϵ . However, if we use the $SU(3)$ relation

$$\frac{P^{(ut)}}{T + P^{(ct)}} = \frac{\tilde{P}^{(ut)}}{\tilde{T} + \tilde{P}^{(ct)}}, \quad (100)$$

where decay constants and form factors cancel in factorisation, we get

$$ae^{i\theta} = \tilde{a}e^{i\tilde{\theta}} \left[\frac{1 + r_{PA}}{1 + x} \right], \quad (101)$$

with

$$r_{PA} \equiv \frac{PA^{(ut)}}{P^{(ut)}}; \quad (102)$$

the parameter x was introduced in Eq. (43). Consequently, we have

$$\frac{1 - \tilde{a}e^{i\tilde{\theta}} e^{i\gamma}}{1 - ae^{i\theta} e^{i\gamma}} = 1 + \mathcal{O}(\tilde{a}x) + \mathcal{O}(\tilde{a}r_{PA}), \quad (103)$$

where the second-order terms are expected to give small corrections at the few-percent level. Introducing the ratio

$$\begin{aligned} & \Xi(B_d \rightarrow D_d^- D_d^+, B_s \rightarrow D_s^- D_d^+) \\ & \equiv \left[\frac{m_{B_d}}{m_{B_s}} \frac{\Phi(m_{D_s}/m_{B_s}, m_{D_d}/m_{B_s}) \tau_{B_s}}{\Phi(m_{D_d}/m_{B_d}, m_{D_d}/m_{B_d}) \tau_{B_d}} \right] \left[\frac{\mathcal{B}(B_d \rightarrow D_d^- D_d^+)}{\mathcal{B}(B_s \rightarrow D_s^- D_d^+)_{\text{theo}}} \right] = 0.59 \pm 0.14, \quad (104) \end{aligned}$$

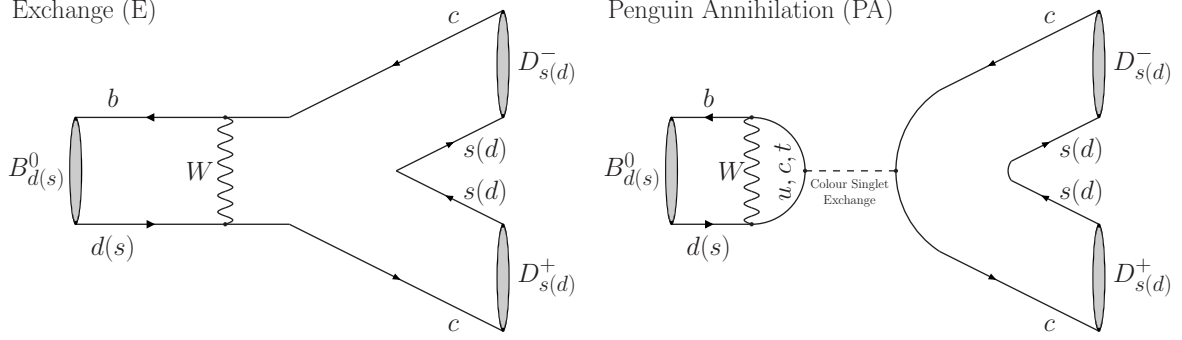


Figure 5: Illustration of exchange and penguin annihilation topologies contributing to $B_d^0 \rightarrow D_s^- D_s^+$ and $B_s^0 \rightarrow D_d^- D_d^+$.

we obtain

$$\Xi(B_d \rightarrow D_d^- D_d^+, B_s \rightarrow D_s^- D_s^+) = |\varrho|^2 + 2|\varrho||\tilde{x}| \cos(\omega - \tilde{\sigma}) + |\tilde{x}|^2 \quad (105)$$

in analogy to Eq. (95).

It is interesting to consider the double ratio

$$\begin{aligned} & \frac{\Xi(B_s \rightarrow D_s^- D_s^+, B_d \rightarrow D_d^- D_d^+)}{\Xi(B_d \rightarrow D_d^- D_d^+, B_s \rightarrow D_s^- D_s^+)} \\ &= \frac{|\varrho'|^2 + 2|\varrho'||\tilde{x}'| \cos(\omega' - \tilde{\sigma}') + |\tilde{x}'|^2}{|\varrho|^2 + 2|\varrho||\tilde{x}| \cos(\omega - \tilde{\sigma}) + |\tilde{x}|^2} \approx \left| \frac{\varrho'}{\varrho} \right|^2 \approx (\varrho'_{\text{fact}})^4 = 1.35 \pm 0.26, \end{aligned} \quad (106)$$

where we have neglected the $|\tilde{x}^{(\prime)}|$ terms and have used Eq. (99). The experimental results in Eqs. (94) and (104) give

$$\frac{\Xi(B_s \rightarrow D_s^- D_s^+, B_d \rightarrow D_d^- D_d^+)}{\Xi(B_d \rightarrow D_d^- D_d^+, B_s \rightarrow D_s^- D_s^+)} = 1.11 \pm 0.28, \quad (107)$$

which is in agreement with the expectation in Eq. (106). The current uncertainties are unfortunately too large to draw any further conclusions.

3.3.3 Probing Exchange and Penguin Annihilation Topologies Directly

The exchange and penguin annihilation topologies can be probed in a *direct* way by means of the decays $B_s^0 \rightarrow D_d^- D_d^+$ and $B_d^0 \rightarrow D_s^- D_s^+$. These modes receive only contributions from exchange and penguin annihilation topologies [7,30], as illustrated in Fig. 5, and are related to each other through the U -spin symmetry. The current experimental information on the corresponding CP-averaged branching ratios is given as follows [1]:

$$\mathcal{B}(B_d \rightarrow D_s^- D_s^+) < 3.6 \times 10^{-5} \text{ (90\% C.L.)}, \quad (108)$$

$$\mathcal{B}(B_s \rightarrow D_d^- D_d^+) = (2.2 \pm 0.6) \times 10^{-4}. \quad (109)$$

The experimental signal for the $B_s^0 \rightarrow D_d^- D_d^+$ decay is in accordance with the picture emerging from the discussion given above.

Let us now have a closer look at these decays. Their amplitudes can be written as

$$A(B_d^0 \rightarrow D_s^- D_s^+) = -\lambda \mathcal{A}_{EPA} [1 - a_{EPA} e^{i\theta_{EPA}} e^{i\gamma}] , \quad (110)$$

$$A(B_s^0 \rightarrow D_d^- D_d^+) = \left(1 - \frac{\lambda^2}{2}\right) \mathcal{A}'_{EPA} [1 + \epsilon a'_{EPA} e^{i\theta'_{EPA}} e^{i\gamma}] , \quad (111)$$

where

$$\mathcal{A}_{EPA} \equiv \lambda^2 A [\hat{E} + \hat{P}A^{(ct)}] , \quad (112)$$

$$\tilde{a}_{EPA} e^{i\tilde{\theta}_{EPA}} \equiv R_b \left[\frac{\hat{P}A^{(ut)}}{\hat{E} + \hat{P}A^{(ct)}} \right] ; \quad (113)$$

the primed parameters are defined in an analogous way. We obtain then

$$\frac{A(B_s^0 \rightarrow D_d^- D_d^+)}{A(B_d^0 \rightarrow D_d^- D_s^+)} = \left(\frac{\mathcal{A}'_{EPA}}{\tilde{\mathcal{A}}'} \right) \left[\frac{1 + \epsilon a'_{EPA} e^{i\theta'_{EPA}} e^{i\gamma}}{1 + \epsilon \tilde{a}' e^{i\tilde{\theta}'} e^{i\gamma}} \right] = \zeta' \tilde{x}' , \quad (114)$$

where we have neglected the terms proportional to the tiny ϵ factor and introduced the parameter

$$\zeta' \equiv \frac{\hat{E}' + \hat{P}A'^{(ct)}}{E' + PA'^{(ct)}} \approx \left(\frac{f_{D_d} m_{D_s}}{m_{D_d} f_{D_s}} \right)^2 = 0.700 \pm 0.042 . \quad (115)$$

In the estimate of this $SU(3)$ -breaking parameter, we have used that exchange and penguin annihilation topologies, which are genuinely of non-factorisable nature, are expected to be suppressed by the smallness of the B - and D -meson wave functions at the origin, which behave as f_B/m_B and f_D/m_D , respectively [66]. The f_{B_s}/m_{B_s} terms cancel in Eq. (115), and the error of the numerical value describing the leading $SU(3)$ -breaking effect corresponds only to the uncertainties of the $D_{d,s}$ -meson decay constants and masses. The ratio⁶

$$\begin{aligned} & \Xi(B_s \rightarrow D_d^- D_d^+, B_d \rightarrow D_d^- D_s^+) \\ & \equiv \left[\frac{m_{B_s}}{m_{B_d}} \frac{\Phi(m_{D_d}/m_{B_d}, m_{D_s}/m_{B_d}) \tau_{B_d}}{\Phi(m_{D_d}/m_{B_s}, m_{D_d}/m_{B_s}) \tau_{B_s}} \right] \left[\frac{\mathcal{B}(B_s \rightarrow D_d^- D_d^+)_{\text{theo}}}{\mathcal{B}(B_d \rightarrow D_d^- D_s^+)} \right] = 0.031 \pm 0.009 \end{aligned} \quad (116)$$

takes then the simple form

$$\Xi(B_s \rightarrow D_d^- D_d^+, B_d \rightarrow D_d^- D_s^+) = |\zeta' \tilde{x}'|^2 , \quad (117)$$

which fixes a circle with radius $|\zeta' \tilde{x}'|$ around the origin in the complex plane.

Concerning the $B_d^0 \rightarrow D_s^- D_s^+$ decay, we have

$$\frac{A(B_d^0 \rightarrow D_s^- D_s^+)}{A(B_s^0 \rightarrow D_s^- D_d^+)} = \left(\frac{\mathcal{A}_{EPA}}{\tilde{\mathcal{A}}'} \right) \left[\frac{1 - a_{EPA} e^{i\theta_{EPA}} e^{i\gamma}}{1 - \tilde{a} e^{i\tilde{\theta}} e^{i\gamma}} \right] = \zeta \tilde{x} , \quad (118)$$

where we have neglected the penguin annihilation contributions on the right-hand side, and have introduced

$$\zeta \equiv \frac{\hat{E} + \hat{P}A^{(ct)}}{E + PA^{(ct)}} \approx \left(\frac{f_{D_s} m_{D_d}}{m_{D_s} f_{D_d}} \right)^2 = 1.408 \pm 0.057 \approx \frac{1}{\zeta'} . \quad (119)$$

⁶We assume $\mathcal{A}_{\Delta\Gamma}(B_s \rightarrow D_d^- D_d^+) = -\cos\phi_s^{\text{SM}}$ for the conversion of the untagged experimental $B_s^0 \rightarrow D_d^- D_d^+$ branching ratio into the corresponding theoretical branching ratio.

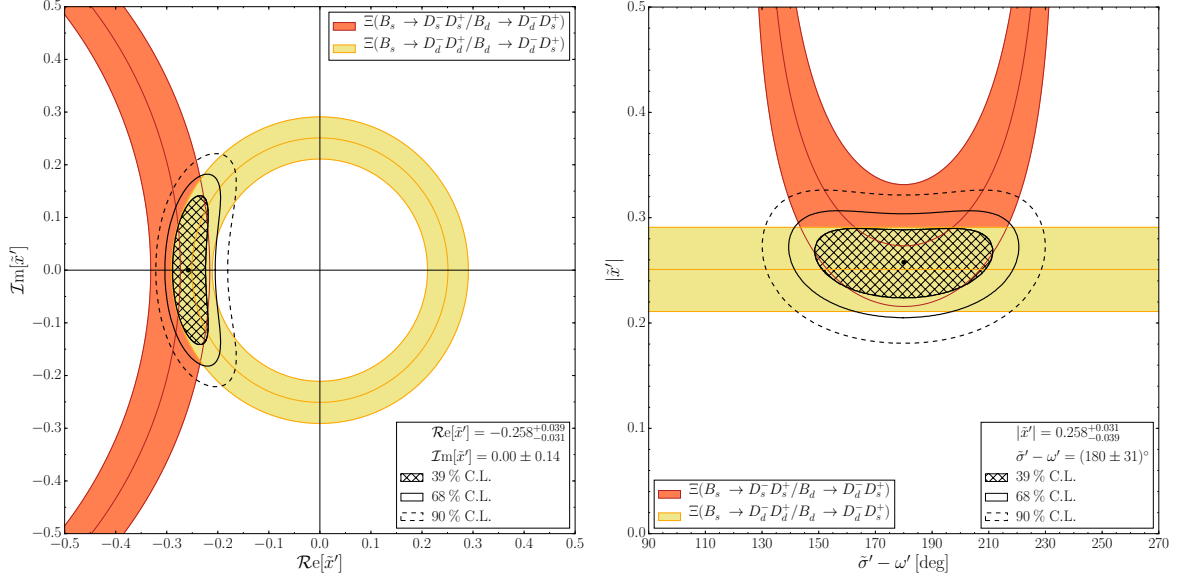


Figure 6: Determination of the parameters $|\tilde{x}'|$ and $\tilde{\sigma}'$ introduced in Eq. (85) from a fit to Eqs. (94) and (116), which characterise the currently available experimental data. For the left plot, a value $\omega' = 0$ is assumed.

As in Eq. (115), we expect that the numerical value describes the leading $SU(3)$ -breaking effect (the uncertainty corresponds only to the decay constants and masses). Non-factorisable $SU(3)$ -breaking contributions to this quantity cannot be estimated at present.

For the comparison with the experimental data we introduce

$$\begin{aligned} & \Xi(B_d \rightarrow D_s^- D_s^+, B_s \rightarrow D_s^- D_d^+) \\ & \equiv \left[\frac{m_{B_d} \Phi(m_{D_s}/m_{B_s}, m_{D_d}/m_{B_s}) \tau_{B_s}}{m_{B_s} \Phi(m_{D_s}/m_{B_d}, m_{D_s}/m_{B_d}) \tau_{B_d}} \right] \left[\frac{\mathcal{B}(B_d \rightarrow D_s^- D_s^+)}{\mathcal{B}(B_s \rightarrow D_s^- D_d^+)_{\text{theo}}} \right] < 0.107 \text{ (90\% C.L.)}, \end{aligned} \quad (120)$$

which takes the simple form

$$\Xi(B_d \rightarrow D_s^- D_s^+, B_s \rightarrow D_s^- D_d^+) = |\zeta \tilde{x}'|^2. \quad (121)$$

Also in this case it is interesting to consider the double ratio

$$\frac{\Xi(B_d \rightarrow D_s^- D_s^+, B_s \rightarrow D_s^- D_d^+)}{\Xi(B_s \rightarrow D_d^- D_d^+, B_d \rightarrow D_d^- D_s^+)} = \left| \frac{\zeta \tilde{x}'}{\zeta' \tilde{x}'} \right|^2, \quad (122)$$

which allows us to test the relation

$$\tilde{x}' \approx \left[\left(\frac{f_{B_s} f_{D_s}}{f_{B_d} f_{D_d}} \right) \varrho'_{\text{fact}} \right] \tilde{x}. \quad (123)$$

Let us now convert the experimental results in Eqs. (94) and (116) into constraints on $|\tilde{x}'|$ and $\tilde{\sigma}'$. While the latter observable simply fixes a circle around the origin in the

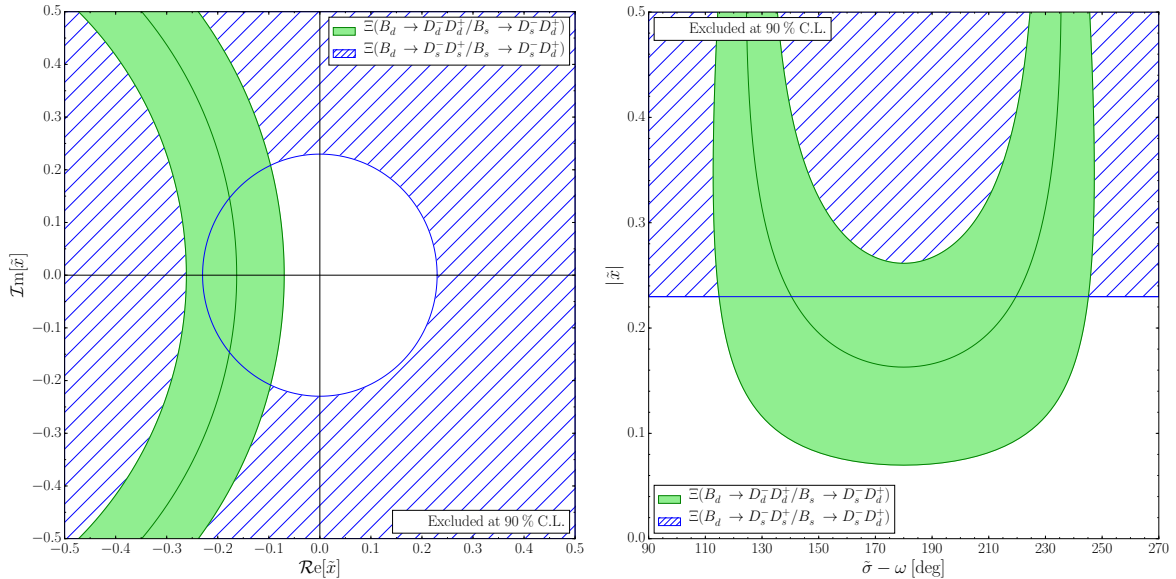


Figure 7: Current experimental constraints, given in Eqs. (104) and (120), on the parameters $|\tilde{x}|$ and $\tilde{\sigma}$ introduced in Eq. (97). For the left plot, a value $\omega' = 0$ is assumed.

complex plane, the former requires information about the $SU(3)$ -breaking parameter ϱ' . We shall use the result in Eq. (93) for our numerical analysis as a guideline. A fit yields

$$\text{Re}(\tilde{x}') = -0.258_{-0.031}^{+0.039}, \quad \text{Im}(\tilde{x}') = 0.0 \pm 0.14, \quad (124)$$

or alternatively

$$|\tilde{x}'| = 0.258_{-0.039}^{+0.031}, \quad \tilde{\sigma}' - \omega' = (180 \pm 34)^\circ, \quad (125)$$

with the corresponding confidence-level contours shown in Fig. 6.

The exchange and penguin annihilation topologies play hence a surprisingly prominent role in the decays at hand, pointing towards large long-distance strong interaction effects. An example of such a contribution to the exchange topology is given by

$$B_s^0 \rightarrow [D_s^- D_s^+, D_s^{*-} D_s^+, \dots] \rightarrow D_d^- D_d^+, \quad (126)$$

as illustrated in the right panel of Fig. 2.

A similar analysis can be performed for the observables in Eqs. (104) and (120), which allow the determination of $|\tilde{x}|$ and $\tilde{\sigma}$. In contrast to the determination of $|\tilde{x}'|$ and $\tilde{\sigma}'$, the penguin effects in the amplitude ratios do not enter with the tiny ϵ and lead to additional uncertainties. In Fig. 7, we show the constraints from the current data, which are still pretty weak. Here we may have long-distance rescattering contributions from processes of the kind

$$B_d^0 \rightarrow [D_d^- D_d^+, D_d^{*-} D_d^+, \dots] \rightarrow D_s^- D_s^+. \quad (127)$$

In the future, following these lines, the comparison between the values of \tilde{x}' and \tilde{x} will offer yet another test of the relation in Eq. (123), going beyond Eq. (122) through information on the strong phases.

3.4 Global Analysis of the Penguin Parameters

3.4.1 Information from Branching Ratios and Non-factorisable Effects

Let us now use the currently available data to constrain the penguin parameters. Unfortunately, a measurement of the differential semileptonic $B_s^0 \rightarrow D_s^- \ell^+ \nu_\ell$ rate is not available. Consequently, we may not yet apply Eq. (45) and have to follow a different avenue, involving larger theoretical uncertainties. In analogy to the H observable defined in Eq. (25), we introduce the following quantities:

$$\tilde{H} \equiv \frac{1}{\epsilon} \left| \frac{\tilde{\mathcal{A}}'}{\tilde{\mathcal{A}}} \right|^2 \left[\frac{m_{B_s}}{m_{B_d}} \frac{\Phi(m_{D_d}/m_{B_d}, m_{D_s}/m_{B_d}) \tau_{B_d}}{\Phi(m_{D_s}/m_{B_s}, m_{D_d}/m_{B_s}) \tau_{B_s}} \right] \frac{\mathcal{B}(B_s \rightarrow D_s^- D_d^+)_{\text{theo}}}{\mathcal{B}(B_d \rightarrow D_d^- D_s^+)}, \quad (128)$$

$$= \frac{1 - 2 \tilde{a} \cos \tilde{\theta} \cos \gamma + \tilde{a}^2}{1 + 2\epsilon \tilde{a}' \cos \tilde{\theta}' \cos \gamma + \epsilon^2 \tilde{a}'^2}, \quad (129)$$

$$H_c \equiv \frac{1}{\epsilon} \left| \frac{\tilde{\mathcal{A}}'_c}{\tilde{\mathcal{A}}_c} \right|^2 \left[\frac{\Phi(m_{D_u}/m_{B^\pm}, m_{D_s}/m_{B^\pm})}{\Phi(m_{D_u}/m_{B^\pm}, m_{D_d}/m_{B^\pm})} \right] \frac{\mathcal{B}(B^\pm \rightarrow D_u D_d^\pm)}{\mathcal{B}(B^\pm \rightarrow D_u D_s^\pm)}, \quad (130)$$

$$= \frac{1 - 2 \tilde{a}_c \cos \tilde{\theta}_c \cos \gamma + \tilde{a}_c^2}{1 + 2\epsilon \tilde{a}'_c \cos \tilde{\theta}'_c \cos \gamma + \epsilon^2 \tilde{a}'_c{}^2}. \quad (131)$$

If we complement \tilde{H} with direct CP violation in $B_s^0 \rightarrow D_s^- D_d^+$ (and the suppressed CP asymmetry in $B_d^0 \rightarrow D_d^- D_s^+$) and H_c with direct CP violation in $B^\pm \rightarrow D_u D_d^\pm$ (and the suppressed CP asymmetry in $B^\pm \rightarrow D_u D_s^\pm$), we may determine the penguin parameters $(\tilde{a}, \tilde{\theta})$ and $(\tilde{a}_c, \tilde{\theta}_c)$, respectively. These determinations are analogous to the determination of (a, θ) from H and the direct CP asymmetry in $B_d^0 \rightarrow D_d^- D_d^+$ (and the suppressed CP asymmetry in $B_s^0 \rightarrow D_s^- D_s^+$). The hence determined parameters offer insights into the r_A and r_{PA} parameters introduced in Eqs. (65) and (102), respectively, and allow for a comparison of the relative non-factorisable contributions.

In contrast to the measurements of the CP asymmetries, the extraction of the H , \tilde{H} and H_c observables from the data requires knowledge of the following amplitude ratios:

$$\frac{\mathcal{A}'}{\mathcal{A}} = \frac{T' + P^{(ct)'} + E' + PA^{(ct)'}}{T + P^{(ct)} + E + PA^{(ct)}} = \left[\frac{T'}{T} \right] \left[\frac{1 + P^{(ct)'} / T'}{1 + P^{(ct)} / T} \right] \left[\frac{1 + x'}{1 + x} \right] \approx \left[\frac{1 + x'}{1 + x} \right] \frac{T'}{T}, \quad (132)$$

$$\frac{\tilde{\mathcal{A}}'}{\tilde{\mathcal{A}}} = \frac{\tilde{T}' + \tilde{P}^{(ct)'}}{\tilde{T} + \tilde{P}^{(ct)}} = \left[\frac{\tilde{T}'}{\tilde{T}} \right] \left[\frac{1 + \tilde{P}^{(ct)'}/\tilde{T}'}{1 + \tilde{P}^{(ct)}/\tilde{T}} \right] \approx \frac{\tilde{T}'}{\tilde{T}}, \quad (133)$$

$$\frac{\tilde{\mathcal{A}}'_c}{\tilde{\mathcal{A}}_c} = \frac{\tilde{T}'_c + \tilde{P}_c^{(ct)'}}{\tilde{T} + \tilde{P}^{(ct)}} = \left[\frac{\tilde{T}'_c}{\tilde{T}_c} \right] \left[\frac{1 + \tilde{P}_c^{(ct)'}/\tilde{T}'_c}{1 + \tilde{P}_c^{(ct)}/\tilde{T}_c} \right] \approx \frac{\tilde{T}'_c}{\tilde{T}_c}. \quad (134)$$

These quantities are governed by U -spin-breaking effects in the ratio of the colour-allowed

tree contributions, which we may write as

$$\left| \frac{T'}{T} \right| = \left[\frac{m_{B_s}^2 - m_{D_s}^2}{m_{B_d}^2 - m_{D_d}^2} \right] \left[\frac{f_{D_s}}{f_{D_d}} \right] \left[\frac{F_0^{B_s D_s}(m_{D_s}^2)}{F_0^{B_d D_d}(m_{D_d}^2)} \right] \left[\frac{a_{\text{NF}}^{T'}}{a_{\text{NF}}^T} \right], \quad (135)$$

$$\left| \frac{\tilde{T}'}{\tilde{T}} \right| = \left[\frac{m_{B_d}^2 - m_{D_d}^2}{m_{B_s}^2 - m_{D_s}^2} \right] \left[\frac{f_{D_s}}{f_{D_d}} \right] \left[\frac{F_0^{B_d D_d}(m_{D_s}^2)}{F_0^{B_s D_s}(m_{D_d}^2)} \right] \left[\frac{\tilde{a}_{\text{NF}}^{T'}}{\tilde{a}_{\text{NF}}^T} \right], \quad (136)$$

$$\left| \frac{\tilde{T}'_c}{\tilde{T}_c} \right| = \left[\frac{f_{D_s}}{f_{D_d}} \right] \left[\frac{\tilde{a}_{\text{NF},c}^{T'}}{\tilde{a}_{\text{NF},c}^T} \right], \quad (137)$$

where the parameters a_{NF}^T describe non-factorisable contributions affecting the colour-allowed tree amplitude (see Eq. (44)). If we assume that all the a_{NF}^T parameters are equal to one another due to the $SU(3)$ flavour symmetry, the following relation can be derived:

$$\left| \frac{T'}{T} \right| \left| \frac{\tilde{T}'}{\tilde{T}} \right| = \left| \frac{\tilde{T}'_c}{\tilde{T}_c} \right|^2, \quad (138)$$

where the decay constants and form factors cancel. In terms of branching ratios, using Eqs. (132)–(134), this relation implies

$$\mathcal{G} \equiv \frac{\mathcal{B}(B^\pm \rightarrow D_u D_d^\pm)}{\mathcal{B}(B^\pm \rightarrow D_u D_s^\pm)} \sqrt{\left[\frac{\mathcal{B}(B_s \rightarrow D_s^- D_s^+)}{\mathcal{B}(B_s \rightarrow D_s^- D_d^+)} \right] \left[\frac{\mathcal{B}(B_d \rightarrow D_d^- D_s^+)}{\mathcal{B}(B_d \rightarrow D_d^- D_d^+)} \right]} \approx 1. \quad (139)$$

The current data give

$$\mathcal{G} = 0.85 \pm 0.16, \quad (140)$$

which is consistent with Eq. (139) within the uncertainties.

Using data for the semileptonic $B_d^0 \rightarrow D_d^- \ell^+ \nu_\ell$ decay, the non-factorisable effects can be probed through

$$\begin{aligned} \tilde{R}_{D_d} &\equiv \frac{\Gamma(B_d^0 \rightarrow D_d^- D_s^+)}{[\text{d}\Gamma(B_d^0 \rightarrow D_d^- \ell^+ \nu_\ell)/\text{d}q^2]_{q^2=m_{D_q}^2}} \\ &= 6\pi^2 |V_{cs}|^2 f_{D_s}^2 X_{B_d D_d}^{D_s} |\tilde{a}'_{\text{NF}}|^2 \left[1 + 2 \epsilon \tilde{a}' \cos \tilde{\theta}' \cos \gamma + \epsilon^2 \tilde{a}'^2 \right], \end{aligned} \quad (141)$$

where

$$X_{B_d D_d}^{D_s} = \frac{(m_{B_d}^2 - m_{D_d}^2)^2}{\left[m_{B_d}^2 - (m_{D_d} + m_{D_s})^2 \right] \left[m_{B_d}^2 - (m_{D_d} - m_{D_s})^2 \right]} \left[\frac{F_0^{B_d D_d}(m_{D_s}^2)}{F_1^{B_d D_d}(m_{D_s}^2)} \right]^2, \quad (142)$$

and

$$\tilde{a}'_{\text{NF}} = \tilde{a}_{\text{NF}}^{T'} [1 + \tilde{r}'_P], \quad (143)$$

with

$$\tilde{r}'_P \equiv \frac{\tilde{P}^{(ct)'}}{\tilde{T}'}, \quad (144)$$

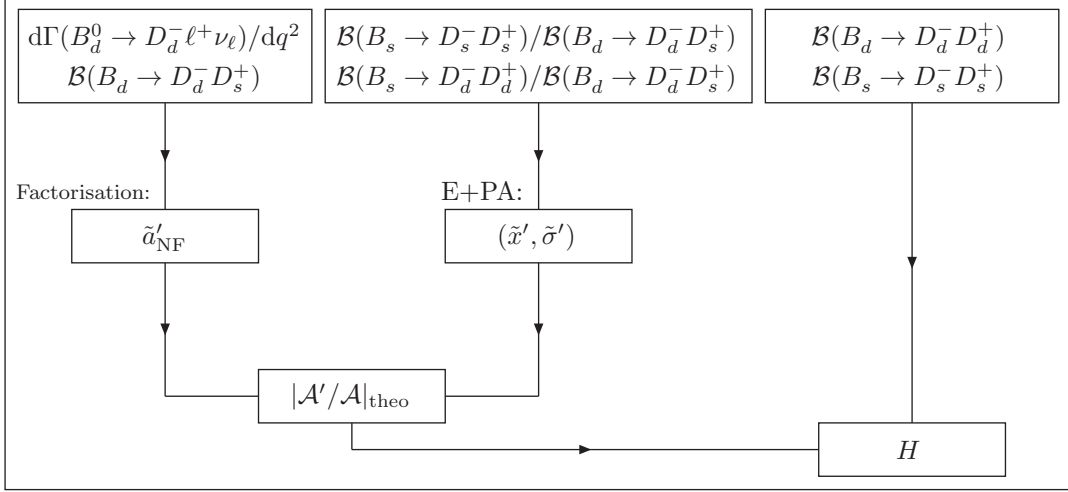


Figure 8: Flow chart illustrating the *classic* strategy to determine H using data from $B \rightarrow D\bar{D}$ branching ratio measurements.

defined in analogy to Eq. (42). Experimentally, we find

$$\tilde{R}_{D_d} = (2.90 \pm 0.41) \text{ GeV}^2, \quad (145)$$

corresponding to a non-factorisable contribution

$$\boxed{|\tilde{a}'_{\text{NF}}| = |\tilde{a}_{\text{NF}}^{T'}| |1 + \tilde{r}'_P| = 0.756 \pm 0.085,} \quad (146)$$

where Eq. (53) has been used for the ratio of form factors. In this result, the penguin effects suppressed by ϵ in Eq. (141) were neglected. It is plausible to interpret the deviation from one at the 2.9σ level as footprints of sizeable penguin effects. We shall discuss this parameter below.

The ratios in Eqs. (132)–(134) can be written in the following forms:

$$\left| \frac{\mathcal{A}'}{\mathcal{A}} \right| = \left| \frac{1+x'}{1+x} \right| \left[\frac{a_{\text{NF}}^{(0)'}}{a_{\text{NF}}^{(0)}} \right] \left| \frac{T'}{T} \right|_{\text{fact}}, \quad (147)$$

$$\left| \frac{\tilde{\mathcal{A}}'}{\tilde{\mathcal{A}}} \right| = \left[\frac{\tilde{a}'_{\text{NF}}}{\tilde{a}_{\text{NF}}} \right] \left| \frac{\tilde{T}'}{\tilde{T}} \right|_{\text{fact}}, \quad (148)$$

$$\left| \frac{\tilde{\mathcal{A}}'_c}{\tilde{\mathcal{A}}_c} \right| = \left[\frac{\tilde{a}'_{\text{NF},c}}{\tilde{a}_{\text{NF},c}} \right] \left| \frac{\tilde{T}'_c}{\tilde{T}_c} \right|_{\text{fact}}, \quad (149)$$

which is also graphically illustrated in Fig. 8. In the above equation, $a_{\text{NF}}^{(0)}$ differs from a_{NF} introduced in Eq. (41) through the $(1+x)$ term, to account for the contributions from exchange and penguin annihilation topologies, which are absent in the decays of the other two ratios. We thus have

$$a_{\text{NF}} = (1+x)a_{\text{NF}}^{(0)}. \quad (150)$$

As in the discussion in Subsection 2.4, it is convenient to write

$$|\tilde{a}'_{\text{NF}}| = 1 + \tilde{\Delta}'_{\text{NF}}, \quad |\tilde{a}_{\text{NF}}| = 1 + \tilde{\Delta}'_{\text{NF}}[1 - \tilde{\xi}_{SU(3)}], \quad (151)$$

where the parameter $\tilde{\xi}_{SU(3)}$ describes $SU(3)$ -breaking effects in the non-factorisable contributions, yielding

$$\left| \frac{\tilde{a}'_{\text{NF}}}{\tilde{a}_{\text{NF}}} \right| = \frac{1 + \tilde{\Delta}'_{\text{NF}}}{1 + \tilde{\Delta}'_{\text{NF}}} = 1 + \tilde{\xi}_{SU(3)} \tilde{\Delta}'_{\text{NF}} + \mathcal{O}(\tilde{\Delta}_{\text{NF}}'^2). \quad (152)$$

Consequently, $\tilde{\Delta}'_{\text{NF}} = -0.244 \pm 0.085$, as determined from Eq. (146), allows us to take non-factorisable corrections to Eqs. (147)–(149) into account, assuming

$$\boxed{\left| \frac{a_{\text{NF}}^{(0)'}}{a_{\text{NF}}^{(0)}} \right| = \left| \frac{\tilde{a}'_{\text{NF}}}{\tilde{a}_{\text{NF}}} \right| = \left| \frac{\tilde{a}'_{\text{NF,c}}}{\tilde{a}_{\text{NF,c}}} \right|}. \quad (153)$$

In these relations, $SU(3)$ -breaking effects enter only through different spectator quarks and are expected to be small.

In order to determine the $SU(3)$ -breaking effects in the ratio of the colour-allowed tree amplitudes $|T'/T|$, we use again Eq. (90) to derive the following expression [5]:

$$\left| \frac{T'}{T} \right|_{\text{fact}} = \left[\frac{m_{B_s}^2 - m_{D_s}^2}{m_{B_d}^2 - m_{D_d}^2} \right] \left[\frac{f_{D_s}}{f_{D_d}} \right] \left[\frac{F_0^{B_s D_s}(m_{D_s}^2)}{F_0^{B_d D_d}(m_{D_d}^2)} \right] = \rho'_{\text{fact}} \left[\frac{f_{D_s}}{f_{D_d}} \right] = 1.356 \pm 0.076. \quad (154)$$

For the calculation of the numerical value, we have used Eq. (92) and the values of the decay constants in Eq. (51). In analogy, we get

$$\left| \frac{\tilde{T}'}{\tilde{T}} \right|_{\text{fact}} = \left[\frac{m_{B_d}^2 - m_{D_d}^2}{m_{B_s}^2 - m_{D_s}^2} \right] \left[\frac{f_{D_s}}{f_{D_d}} \right] \left[\frac{F_0^{B_d D_d}(m_{D_d}^2)}{F_0^{B_s D_s}(m_{D_s}^2)} \right] = \rho_{\text{fact}} \left[\frac{f_{D_s}}{f_{D_d}} \right] = 1.167 \pm 0.066. \quad (155)$$

In the case of the charged decays, a particularly simple situation arises in factorisation as the form factors cancel:

$$\left| \frac{\tilde{T}'_c}{\tilde{T}_c} \right|_{\text{fact}} = \frac{f_{D_s}}{f_{D_d}}, \quad (156)$$

as is also evident from Eq. (137).

Using the amplitude ratio in Eq. (147), we can now determine the observable H (see Eq. (25)). For this, we also have to quantify the uncertainty from the $SU(3)$ -breaking corrections to the term involving the x and x' parameters. The analysis discussed in Subsection 3.3.2 allows us to accomplish this task. Using the results for \tilde{x}' and $\tilde{\sigma}'$ in Eq. (125) and the relations

$$x' = \frac{\tilde{x}'}{\varrho'}, \quad x \approx \left(\frac{m_{B_s} m_{D_s}}{m_{B_d} m_{D_d}} \right) \left(\frac{f_{B_d} f_{D_d}}{f_{B_s} f_{D_s}} \right) \tilde{x}', \quad (157)$$

yields

$$\left| \frac{1 + x'}{1 + x} \right| = 0.930 \pm 0.020. \quad (158)$$

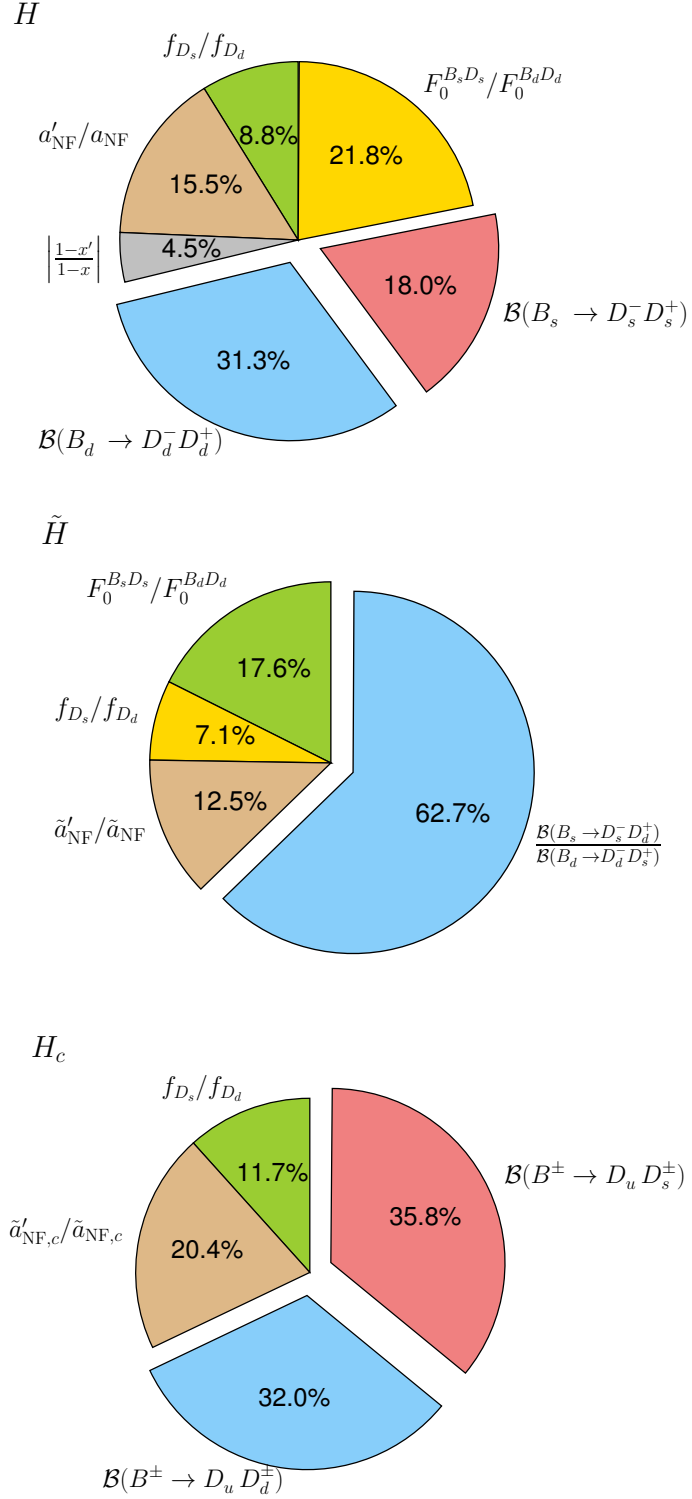


Figure 9: Pie charts illustrating the uncertainty budget of the H observables.

Finally, we obtain

$$\left| \frac{\mathcal{A}'}{\mathcal{A}} \right| = 1.261 \pm 0.091, \quad (159)$$

$$\left| \frac{\tilde{\mathcal{A}}'}{\tilde{\mathcal{A}}} \right| = 1.167 \pm 0.081, \quad (160)$$

$$\left| \frac{\tilde{\mathcal{A}}'_c}{\tilde{\mathcal{A}}_c} \right| = 1.258 \pm 0.063, \quad (161)$$

and correspondingly

$$H = 1.30 \pm 0.26, \quad (162)$$

$$\tilde{H} = 1.28 \pm 0.29, \quad (163)$$

$$H_c = 1.18 \pm 0.21. \quad (164)$$

In Fig. 9 we show the corresponding uncertainty budgets. Should the relations in Eq. (153) actually receive corrections, they would affect this error budget. In the future, implementing the strategy proposed in Section 2.4, this approximation/assumption is no longer needed.

The result on H allows us to put first constraints on the penguin parameters a with the help of the lower bound in Eq. (32):

$$\boxed{a \geq 0.052}, \quad (165)$$

where we have used the lower value of H at one standard deviation.

3.4.2 Information from CP Asymmetries

Let us now add experimental information on CP violation to our analysis. Concerning the decay $B_d^0 \rightarrow D_d^- D_d^+$, the current status of the measurement of the direct and mixing-induced CP asymmetries is given as follows:

$$\mathcal{A}_{\text{CP}}^{\text{dir}}(B_d \rightarrow D_d^- D_d^+) = \begin{cases} -0.07 \pm 0.23 \pm 0.03 & (\text{BaBar [67]}) \\ -0.43 \pm 0.16 \pm 0.05 & (\text{Belle [68]}), \end{cases} \quad (166)$$

$$\mathcal{A}_{\text{CP}}^{\text{mix}}(B_d \rightarrow D_d^- D_d^+) = \begin{cases} +0.63 \pm 0.36 \pm 0.05 & (\text{BaBar [67]}) \\ +1.06_{-0.21}^{+0.14} \pm 0.08 & (\text{Belle [68]}). \end{cases} \quad (167)$$

The measurements by the BaBar and Belle collaborations are not in good agreement with one another, in particular for the mixing-induced CP asymmetry. HFAG gives the following averages [2]:

$$\mathcal{A}_{\text{CP}}^{\text{dir}}(B_d \rightarrow D_d^- D_d^+) = -0.31 \pm 0.14, \quad \mathcal{A}_{\text{CP}}^{\text{mix}}(B_d \rightarrow D_d^- D_d^+) = 0.98 \pm 0.17, \quad (168)$$

which have to be taken with great care. It is nevertheless interesting to use these results as input for the strategy discussed above. A χ^2 fit to Eq. (168) and the value of H in Eq. (162) yields $\chi_{\text{min}}^2 = 0.028$ for 4 degrees of freedom ($a, \theta, \phi_d, \gamma$), and results in the solution

$$\mathcal{R}e[a] = -0.29_{-0.20}^{+0.27}, \quad \mathcal{I}m[a] = -0.204_{-0.105}^{+0.094}, \quad (169)$$

corresponding to

$$\boxed{a = 0.35_{-0.20}^{+0.19}, \quad \theta = (215_{-17}^{+51})^\circ}, \quad (170)$$

and

$$\boxed{\phi_d = (60_{-39}^{+43})^\circ}. \quad (171)$$

Following Refs. [11, 16], we illustrate the various constraints entering the fit through contour bands of the individual observables in Fig. 10. For the $\mathcal{A}_{\text{CP}}^{\text{mix}}(B_d \rightarrow D_d^- D_d^+)$ range, we have used the value of ϕ_d in Eq. (171). The penguin parameters in Eq. (170) result in the penguin phase shift

$$\Delta\phi_d^{D_d^- D_d^+} = (30_{-32}^{+23})^\circ. \quad (172)$$

For the fit, we use the expressions for the CP asymmetries in Eqs. (10) and (11), and the expression for H in Eq. (29) with the U -spin relation in Eq. (7). Since a' enters Eq. (29) with the tiny ϵ , U -spin-breaking corrections to Eq. (7) have a very minor impact.

Although the uncertainties are large, the results from the fit may indicate significant penguin contributions. Should this actually be the case, long-distance effects, such as those illustrated in Fig. 2, would be at work in the penguin sector of the $B_q^0 \rightarrow D_q^- D_q^+$ decays. It is interesting to have a closer look at the result of non-factorisable contributions to $B_d \rightarrow D_d^- D_s^+$ in Eq. (146). It corresponds to

$$|1 + \tilde{r}'_P| = (0.750 \pm 0.055)/|\tilde{a}_{\text{NF}}^{T'}|. \quad (173)$$

Assuming that $|\tilde{a}_{\text{NF}}^{T'}| = 1$, i.e. that the colour-allowed tree topologies have negligible non-factorisable contributions, and that all parameters are real, this results in

$$\tilde{r}'_P = -0.250 \pm 0.055. \quad (174)$$

Note that the uncertainty on \tilde{r}'_P only reflects the uncertainty on the input quantity (146), but does not take into account further theoretical uncertainties associated with the made approximation. Further assuming $\tilde{P}^{(ut)'} = \tilde{P}^{(ct)'}$, which leads to the approximation $ae^{i\theta} \approx R_b \tilde{r}'_P / (1 + \tilde{r}'_P)$, we obtain

$$a = 0.130 \pm 0.039, \quad \theta \sim 180^\circ, \quad (175)$$

which is in the ballpark of the theoretical estimate in Eq. (22). Consequently, it is still premature to draw definite conclusions on anomalously enhanced penguin contributions at this point and future analyses are required to shed light on this issue.

Large penguins would have important consequences for the determination of the B_s^0 - \bar{B}_s^0 mixing phase ϕ_s from the mixing-induced CP violation of the $B_s^0 \rightarrow D_s^- D_s^+$ decay. The LHCb collaboration has recently presented the first analysis of CP violation in this channel [69], yielding

$$\phi_{s, D_s^- D_s^+}^{\text{eff}} = (1.1 \pm 9.7 \pm 1.1)^\circ, \quad |\lambda_{D_s^- D_s^+}| = 0.91 \pm 0.18 \pm 0.02, \quad (176)$$

which can be converted into

$$\mathcal{A}_{\text{CP}}^{\text{dir}}(B_s \rightarrow D_s^- D_s^+) = 0.09 \pm 0.20, \quad \mathcal{A}_{\text{CP}}^{\text{mix}}(B_s \rightarrow D_s^- D_s^+) = 0.02 \pm 0.17. \quad (177)$$

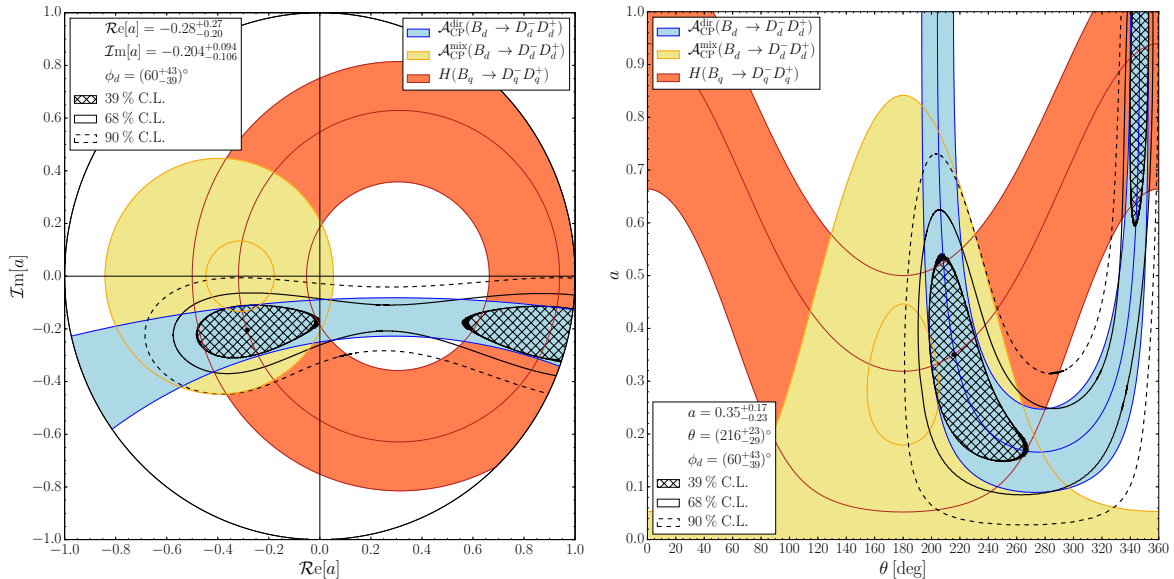


Figure 10: Illustration of the determination of the penguin parameters a and θ from a χ^2 fit to the CP asymmetries of the decay $B_d^0 \rightarrow D_d^- D_d^+$ and the observable H .

These results are in good agreement with the predictions based on a global $SU(3)$ analysis of the $B \rightarrow D\bar{D}$ system [70]. Moreover, we obtain

$$\mathcal{A}_{\Delta\Gamma}(B_s \rightarrow D_s^- D_s^+) = -0.995 \pm 0.019, \quad (178)$$

which should be compared with Eq. (28) corresponding to the direct measurement of the effective lifetime $\tau_{D_s^- D_s^+}^{\text{eff}}$.

If we generalise the U -spin relation in (7) as

$$a' = \xi a, \quad \theta' = \theta + \delta, \quad (179)$$

with the assumed U -spin-breaking parameters $\xi = 1.00 \pm 0.20$ and $\delta = (0 \pm 20)^\circ$ (which are of similar size as the corresponding parameters in Ref. [16]) and use the expression in Eq. (19), the penguin parameters in Eq. (170) determined from the fit can be converted into

$$\Delta\phi_s^{D_s^- D_s^+} = - (1.7^{+1.6}_{-1.2} (\text{stat})^{+0.3}_{-0.7} (U\text{-spin}))^\circ. \quad (180)$$

Finally, we can extract ϕ_s from the effective mixing phase in Eq. (176), which yields

$$\phi_s = - (0.6^{+9.8}_{-9.9} (\text{stat})^{+0.3}_{-0.7} (U\text{-spin}))^\circ. \quad (181)$$

Despite the suppression through the parameter ϵ , penguins may have a significant impact on the extraction of ϕ_s and have to be taken into account. This will be particularly relevant for the LHCb upgrade era. In this new round of precision, we will also get valuable insights into the validity of the U -spin symmetry, parameterised through Eq. (179).

Unfortunately, there is no measurement of CP violation in $B_s^0 \rightarrow D_s^- D_d^+$ available, which would be very interesting, in particular in view of the situation for $B_d^0 \rightarrow D_d^- D_d^+$. Consequently, we may not yet determine \tilde{a} and $\tilde{\theta}$ from the data.

However, for the charged $B^+ \rightarrow \bar{D}^0 D_d^+$ decay, the PDG gives

$$\mathcal{A}_{\text{CP}}^{\text{dir}}(B^\pm \rightarrow D_u D_d^\pm) = +0.03 \pm 0.07. \quad (182)$$

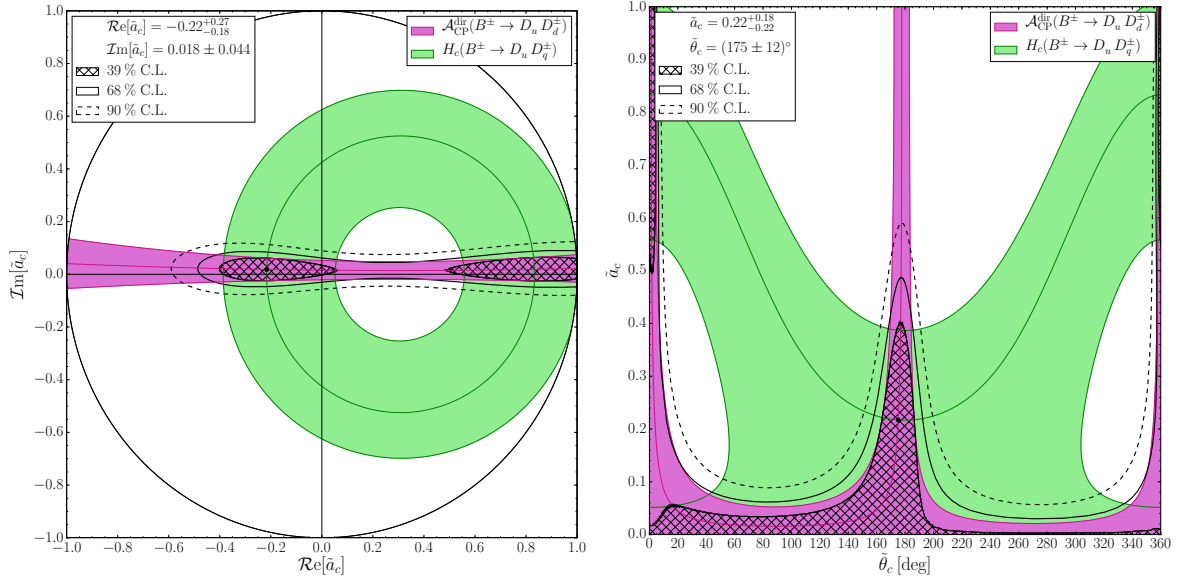


Figure 11: Illustration of the determination of the penguin parameters \tilde{a}_c and $\tilde{\theta}_c$ from a χ^2 fit to the direct CP asymmetries of the decay $B^+ \rightarrow \bar{D}^0 D_d^+$ and the observable H_c .

If we complement this measurement with the value of H_c in Eq. (164), we may perform a fit to the charged decays. It has three degrees of freedom (a, θ, γ), and results in the solution

$$\mathcal{R}e[\tilde{a}_c] = -0.22^{+0.27}_{-0.18}, \quad \mathcal{I}m[\tilde{a}_c] = 0.018 \pm 0.044, \quad (183)$$

which corresponds to

$$\tilde{a}_c = 0.22^{+0.18}_{-0.22}, \quad \tilde{\theta}_c = (175 \pm 12)^\circ. \quad (184)$$

In Fig. 11, we illustrate the corresponding situation, which complements Fig. 10.

It is interesting to compare the penguin parameter $ae^{i\theta}$ with its charged decay counterpart $\tilde{a}_c e^{i\tilde{\theta}_c}$. We obtain

$$r_{PA}^A \equiv \left[\frac{1}{1+x} \right] \left[\frac{\tilde{a}_c e^{i\tilde{\theta}_c}}{ae^{i\theta}} \right] = \frac{1+r_A}{1+r_{PA}}, \quad (185)$$

where we have used Eqs. (64) and (101). The precision that can be obtained with the current data does not yet allow us to draw any conclusions regarding r_{PA}^A . However, in the future it will be interesting to monitor this quantity as the experimental precision improves. Moreover, a measurement of the direct CP violation in the $B_s^0 \rightarrow D_s^- D_d^+$ channel will allow us to determine $\tilde{a}_c e^{i\tilde{\theta}_c}$ from the information from \tilde{H} . The comparison with $\tilde{a}_c e^{i\tilde{\theta}_c}$ will yield the r_A parameter from Eq. (64), so that Eq. (185) will then allow the determination of r_{PA} . Consequently, following these lines, we may reveal the impact of the annihilation and penguin annihilation topologies in the decays at hand.

4 Prospects for the LHCb Upgrade and Belle II Era

Let us conclude the discussion on the $B \rightarrow D\bar{D}$ decays by exploring the potential of these decay modes in the Belle II era and at the LHCb upgrade. We do this using several

scenarios, examined in Section 4.3, that reflect the different possibilities still allowed by the current data. The inputs used in these scenarios are discussed first. Section 4.1 gives the experimental prospects for the relevant CP and branching ratio information of the $B \rightarrow D\bar{D}$ decays, while Section 4.2 deals with the future constraints on the additional decay topologies.

4.1 Extrapolating from Current Results

The B -factories have pioneered the study of $B \rightarrow D\bar{D}$ decays, including the discoveries of numerous $B \rightarrow D\bar{D}$ decay modes [71], the measurements of branching fractions [72, 73], and the analyses of CP asymmetries [67, 68, 72]. The LHCb collaboration subsequently continued the study of $B \rightarrow D\bar{D}$ decays, notably focusing on the analysis of B_s^0 decays [40, 61, 69], which are abundantly produced at the LHC. Based on the successful performance of LHCb during run I of the LHC, an estimate can be made of its performance with the data samples that are expected to be collected after the upgrade of the LHCb detector. For these extrapolations, an integrated luminosity of 5 fb^{-1} in run II, from 2015 until 2018, is assumed. In addition, the B production cross section will increase at a centre-of-mass energy of 13 TeV compared to 8 TeV by about 60%. For the upgrade scenario, an integrated luminosity of 50 fb^{-1} is assumed with increased trigger efficiency, leading to about a three times larger data sample per fb^{-1} compared to the B yield per fb^{-1} at run I. Similarly, a prognosis can be made for measurements at Belle II, which is expected to start taking data in 2018. Here we assume that 50 times more data will be collected than currently is available (1 ab^{-1}).

The expectations for the CP asymmetry parameters are listed in Table 2. The extrapolations are done for the currently available measurements only; no attempt is made to forecast the precision on yet-to-be-performed analyses. For example, the LHCb collaboration will also determine the CP asymmetries of the $B_d^0 \rightarrow D_d^- D_d^+$ decay, but it remains to be seen what the accuracy will be in comparison with possible Belle II results.

The expectations for the branching fractions are listed in Table 3. The ‘‘current measurement’’ column reflects the best available knowledge at this moment, which in some cases could have been more precise if the ratio of branching fractions were determined directly, rather than dividing the individually measured branching fractions. In the extrapolations it is assumed that the ratios of branching fractions are determined. Moreover, it is assumed that the systematic uncertainties due to f_s/f_d (4.7%), due to the D -meson branching fractions (3.9%, 2.1% and 1.3% for D_s^+ , D_d^+ and D^0 mesons, respectively) and due to the different B_s^0 lifetimes (2.9% (1.5%) for a CP (flavour) eigenstate), remain the same. We assume that the total experimental systematic uncertainty

Observable	Current Measurement	Upgrade	Experiment
$\mathcal{A}_{CP}^{\text{dir}}(B_d \rightarrow D_d^- D_d^+)$	$-0.43 \pm 0.16 \pm 0.05$ [68]	± 0.05	Belle
$\mathcal{A}_{CP}^{\text{mix}}(B_d \rightarrow D_d^- D_d^+)$	$1.06 \begin{smallmatrix} +0.14 \\ -0.21 \end{smallmatrix} \pm 0.08$ [68]	± 0.08	Belle
$\mathcal{A}_{CP}^{\text{dir}}(B^\pm \rightarrow D_u D_{(s)}^\pm)$	$0.00 \pm 0.08 \pm 0.02$ [72]	± 0.02	Belle
$\phi_s^{\text{eff}}(B_s \rightarrow D_s^- D_s^+)$	$(1 \pm 10 \pm 1)^\circ$ [69]	$\pm 2^\circ$	LHCb

Table 2: Experimental prospects for the currently available CP asymmetry measurements of $B \rightarrow D\bar{D}$ decays from Belle and LHCb.

Obs	Decay Ratio	Current Measurement of ratio of BRs	LHCb Uncertainty	
			2011	Upgrade
H	$B_d^0 \rightarrow D_d^- D_d^+ / B_s^0 \rightarrow D_s^- D_s^+$	0.048 ± 0.007 [1]	14%(12%)	8%
\tilde{H}	$B_s^0 \rightarrow D_s^- D_d^+ / B_d^0 \rightarrow D_d^- D_s^+$	$0.050 \pm 0.008 \pm 0.004$ [61]	18%	7%
H_c	$B^+ \rightarrow \bar{D}^0 D_d^+ / B^+ \rightarrow \bar{D}^0 D_s^+$	0.042 ± 0.006 [1]	15%(7%)	6%
Ξ	$B_s^0 \rightarrow D_s^- D_s^+ / B_d^0 \rightarrow D_d^- D_s^+$	$0.56 \pm 0.03 \pm 0.04$ [61]	9%	7%
Ξ	$B_d^0 \rightarrow D_d^- D_d^+ / B_s^0 \rightarrow D_s^- D_d^+$	0.59 ± 0.14 [1]	24%(20%)	6%
Ξ	$B_s^0 \rightarrow D_d^- D_d^+ / B_d^0 \rightarrow D_d^- D_s^+$	0.031 ± 0.009 [1]	24%(20%)	11%
Ξ	$B_d^0 \rightarrow D_s^- D_s^+ / B_s^0 \rightarrow D_s^- D_d^+$	Not observed		

Table 3: Experimental prospects for ratios of branching fractions. The second and fourth ratios are obtained from direct determinations of the ratios of branching fractions, whereas the others are calculated from individual branching fractions. The value in brackets indicates the possible uncertainty if this ratio were determined directly. Note that for the calculation of the H observables, additional uncertainties due to $|\mathcal{A}'/\mathcal{A}|$ arise.

Observable	Current Measurement	Upgrade
f_{D_d}	$(204.6 \pm 5.7 \pm 2.0)$ MeV [74]	± 3.0 MeV [75]
f_{D_s}	$(255.5 \pm 4.2 \pm 5.1)$ MeV [76]	± 3.6 MeV*
γ	$(68.3 \pm 7.5)^\circ$ [60]	$\pm 0.9^\circ$ [3]

Table 4: Experimental prospects for external input. A * indicates an average of the extrapolated measurement with the current PDG average.

will decrease from 5.0% to 4.0%. In some ratios, the uncertainty on the D branching fractions cancels with their contribution to the f_s/f_d uncertainty. This is taken into account where appropriate. In our upgrade era scenario, systematic uncertainties will be the limiting factor on the ratio of branching fractions. Therefore, we would like to encourage research into f_s/f_d , $\mathcal{B}(D_s^+ \rightarrow K^+ K^- \pi^+) / \mathcal{B}(D_d^+ \rightarrow K^- \pi^+ \pi^+)$ and B lifetime differences. If these three factors could be reduced to a level of about 2%, then that would lead to a systematic uncertainty of (5–6)% for all of these decays, assuming an experimental uncertainty of 4%. Finally, the prospects for improvements on external input parameters are listed in Table 4.

4.2 Exchange and Penguin Annihilation Contributions

For the construction of the H observable based on the ratio of hadronic amplitudes in Eq. (147), the contributions from exchange and penguin annihilation topologies, represented by the parameters \tilde{x}' and $\tilde{\sigma}'$, need to be quantified. With future, improved measurements of the $B \rightarrow D\bar{D}$ branching ratios it is expected that the picture emerging from the current data, discussed in Section 3.3.2, can be sharpened further. We therefore explore the precision that can be achieved towards the end of the Belle II era and of the LHCb upgrade. Based on the best fit solution obtained from the current data, i.e.

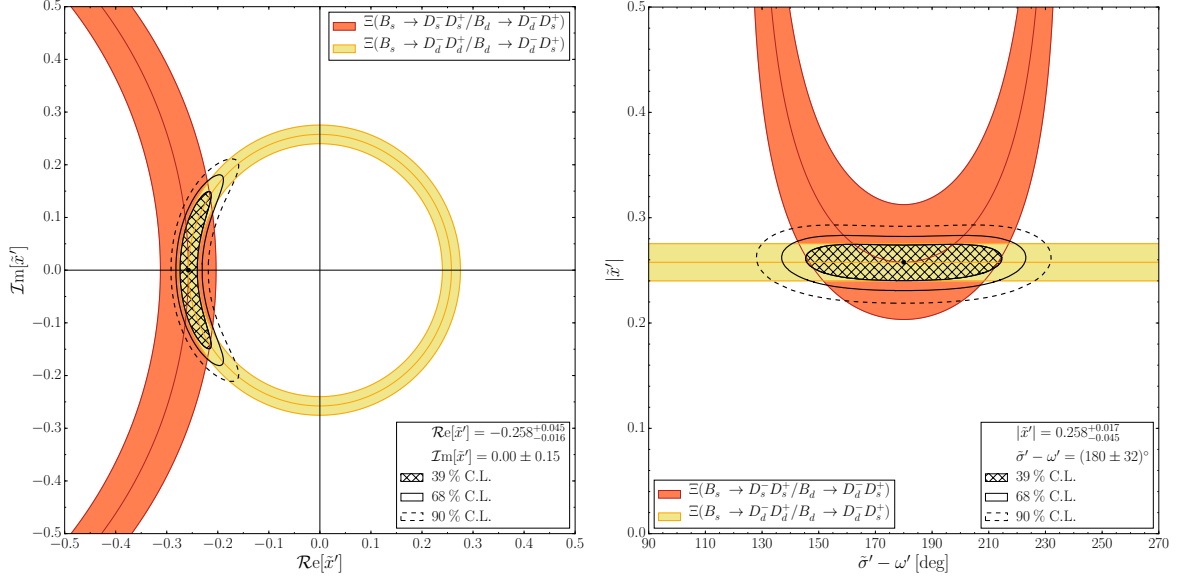


Figure 12: Illustration of the determination of exchange and penguin-annihilation contributions through the parameter x (Eq. (43)) in the Belle II/LHCb upgrade era. The precision should be compared to Fig. 6.

Eq. (125), and the prospects in Table 3, we start from the following input measurements:

$$\Xi(B_s \rightarrow D_s^- D_s^+, B_d \rightarrow D_d^- D_s^+) = 0.673 \pm 0.043, \quad (186)$$

$$\Xi(B_s \rightarrow D_d^- D_d^+, B_d \rightarrow D_d^- D_s^+) = 0.033 \pm 0.004. \quad (187)$$

A fit yields

$$\text{Re}[\tilde{x}'] = -0.258^{+0.045}_{-0.016}, \quad \text{Im}[\tilde{x}'] = 0.00 \pm 0.15, \quad (188)$$

corresponding to

$$\tilde{x}' = 0.258^{+0.017}_{-0.045}, \quad \tilde{\sigma}' - \omega' = (180 \pm 15)^\circ. \quad (189)$$

The associated confidence-level contours are shown in Fig. 12. Note that at first sight these uncertainties do not seem to have improved significantly with respect to the present experimental situation. However, this is merely caused by the shape of the confidence contour in Fig. 12.

4.3 Future Scenarios

To achieve the smallest theoretical uncertainty on the H observable, it should be constructed from the semileptonic decay information, see Eq. (45), as explained in Section 2.4. This method is preferred over the direct ratio of hadronic branching fractions in Eq. (25), as it does not rely on form factor information, and is not experimentally limited by f_s/f_d . However, as the necessary information on $d\Gamma/dq^2(B_s^0 \rightarrow D_s^- \ell^+ \nu_\ell)$ is currently not yet available, we also do not have any estimates for the precision that can be achieved at LHCb or Belle II. For the following discussion, we will thus, like for the fits to the current data, rely on the original definition using the ratio of hadronic branching fractions, Eq. (25).

Using the currently available data, we have illustrated in Section 3.4 that it is possible to simultaneously determine the penguin contributions and the $B_d^0\text{-}\bar{B}_d^0$ mixing phase ϕ_d using the CP and branching ratio information of the $B_d^0 \rightarrow D_d^- D_d^+$ decay. However, as the result of ϕ_d in Eq. (171) shows, the precision on ϕ_d is very limited. Also for the Belle II and LHCb upgrade era it will be challenging to reach precisions below the $(10\text{--}20)^\circ$ level. A high-precision determination of ϕ_d using the $B_d^0 \rightarrow D_d^- D_d^+$ decay is only possible if the direct CP asymmetry and the H observable together are sufficient to unambiguously pin down the penguin parameters a and θ . In such a situation, the phase ϕ_d can then be determined from the mixing-induced CP asymmetry. As Fig. 10 illustrates, a and θ cannot precisely be determined. The situation would arise either for very large values of a , which looks unrealistic, or if the H observable can be determined with a precision of well below the 5% level, which in view of the prospects in Table 3 is unlikely. The determination of ϕ_d from the $B_d^0 \rightarrow D_d^- D_d^+$ decay is therefore not competitive with the results from the $B_d^0 \rightarrow J/\psi K_s^0$ decay. It is thus advantageous to use external input on ϕ_d for the analysis of the $B \rightarrow D\bar{D}$ decays. This extra information breaks the ambiguity that is still present in the confidence-level contours shown in Fig. 10, and can therefore improve the precision on a and θ , and thus also on $\Delta\phi_s$. For the future benchmark scenarios we therefore only focus on the high precision determination of ϕ_s .

Using external input for ϕ_d in principle makes one of the three observables used by the fit ($\mathcal{A}_{\text{CP}}^{\text{dir}}$, $\mathcal{A}_{\text{CP}}^{\text{mix}}$ or H) superfluous. As the H observable receives corrections from possible U -spin-breaking effects through $|\mathcal{A}'/\mathcal{A}|$, which result in large theoretical uncertainties, it is preferred to determine the penguin parameters using information on the CP asymmetries only, omitting H . Such a determination is *theoretically clean*. This will ultimately lead to the highest precision on a , θ and $\Delta\phi_s$. In this situation, the branching ratio information can instead be used to gain insight into the hadronic physics of the $B_d^0 \rightarrow D_d^- D_d^+$, $B_s^0 \rightarrow D_s^- D_s^+$ system. We can then follow the opposite path where the fit results for a and θ can be used to determine the H observable with the help of Eq. (29), labelled $H_{(a,\theta)}$ below. Since a' enters there with the tiny ϵ , the U -spin-breaking corrections affecting the U -spin relation in Eq. (179) have a very minor impact. Since we now know the value of H , the relation (25) can be inverted to instead determine the ratio of hadronic amplitudes

$$\left| \frac{\mathcal{A}'}{\mathcal{A}} \right| = \sqrt{\epsilon H_{(a,\theta)} \left[\frac{m_{B_s}}{m_{B_d}} \frac{\Phi(m_{D_d^-}/m_{B_d}, m_{D_d^+}/m_{B_d}) \tau_{B_d^0}}{m_{B_d} \Phi(m_{D_s^-}/m_{B_s}, m_{D_s^+}/m_{B_s}) \tau_{B_s^0}} \right] \frac{\mathcal{B}(B_s \rightarrow D_s^- D_s^+)_{\text{theo}}}{\mathcal{B}(B_d \rightarrow D_d^- D_d^+)}} \quad (190)$$

from the measured ratio of branching ratios. This experimental measurement of the ratio of hadronic amplitudes can be compared with the theoretical result in Eq. (159). This favourable strategy is illustrated by the flow chart in Fig. 13.

However, the ideal scenario described above cannot always be realised. When the value of the mixing-induced CP asymmetry is compatible with 1 (at the 1σ level), its power to constrain the penguin parameters a and θ is limited. This can best be illustrated using the contour plots, like Fig. 10 or Fig. 17 below. In this situation, the annular constraint originating from the mixing-induced CP asymmetry becomes a closed disk, leading to a large overlap region with the direct CP asymmetry constraint. Consequently, it is not possible to conclusively pin down a and θ in such a situation. Additional information is thus needed to improve the picture, and reach our target of matching the

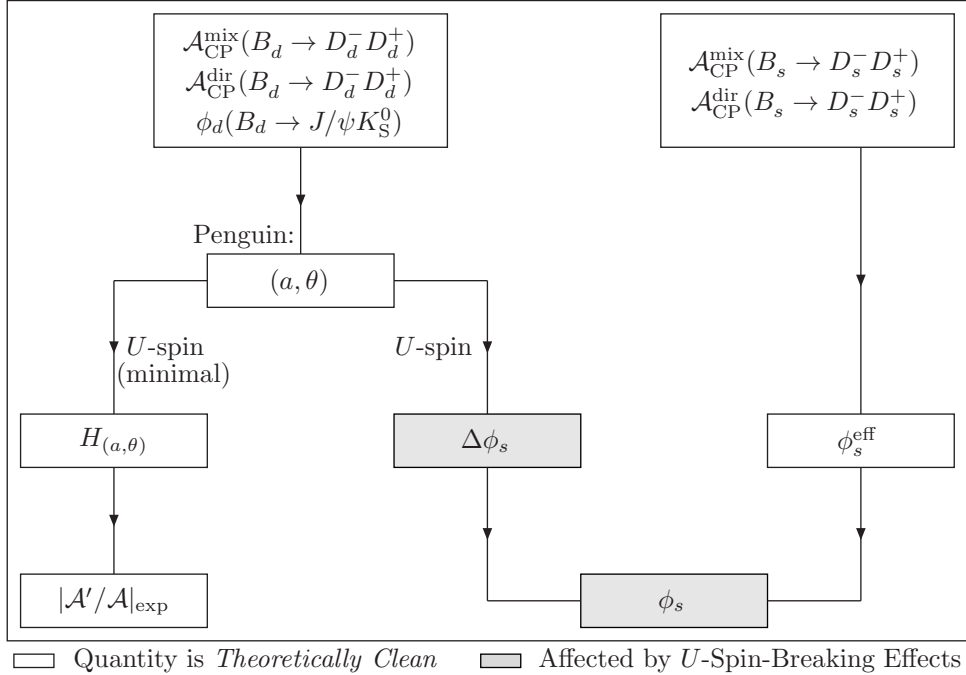


Figure 13: Flow chart illustrating the favourable strategy to control $\Delta\phi_s$, which only requires information on the $B_d^0 \rightarrow D_d^- D_d^+$ CP asymmetries.

foreseen experimental precision on ϕ_s with an equally precise determination of $\Delta\phi_s$. In this situation, the H observable forms an essential ingredient in the fit, and it can therefore not be used to experimentally constrain the ratio of hadronic amplitudes. This less favourable strategy is illustrated by the flow chart in Fig. 14.

Given the current experimental situation, either of the two situations sketched above can still be realised, depending on the future world average for $\mathcal{A}_{\text{CP}}^{\text{mix}}(B_d^0 \rightarrow D_d^- D_d^+)$. To demonstrate the variety of situations in which we may ultimately end up, we made an overview of six different scenarios, covering both situations. Scenarios 1–3 represent the favourable situation in which the H observable can be omitted from the fit, in which we can determine a and θ in a theoretical clean way, and get experimental access to the ratio of hadronic amplitudes. Scenarios 4–6, on the other hand, fall in the second category and do require information on H to conclusively pin down a and θ . All six scenarios are chosen to be compatible with the current experimental situation, with scenario 5 representing the current best fit point, and have $a < R_b$, which is suggested by Eq. (3). Although it is mathematically possible for a to be larger than R_b , it would imply that the penguin topologies are larger than the tree contribution, which seems very unlikely. The condition $a = R_b$ thus serves as a naturally upper limit for the size of the penguin contributions. The different scenarios we consider, and the resulting input values of the three observables ($\mathcal{A}_{\text{CP}}^{\text{dir}}$, $\mathcal{A}_{\text{CP}}^{\text{mix}}$ and H) are listed in Table 5. The choice of input points can be compared with the current fit solution for a and θ in Fig. 15, and with the current measurements of the $B_d^0 \rightarrow D_d^- D_d^+$ CP asymmetry parameters in Fig. 16.

For each of the six scenarios, the individual constraints coming from $\mathcal{A}_{\text{CP}}^{\text{dir}}$, $\mathcal{A}_{\text{CP}}^{\text{mix}}$ and H are illustrated in Fig. 17. The three left-most plots represent the favourable situation,

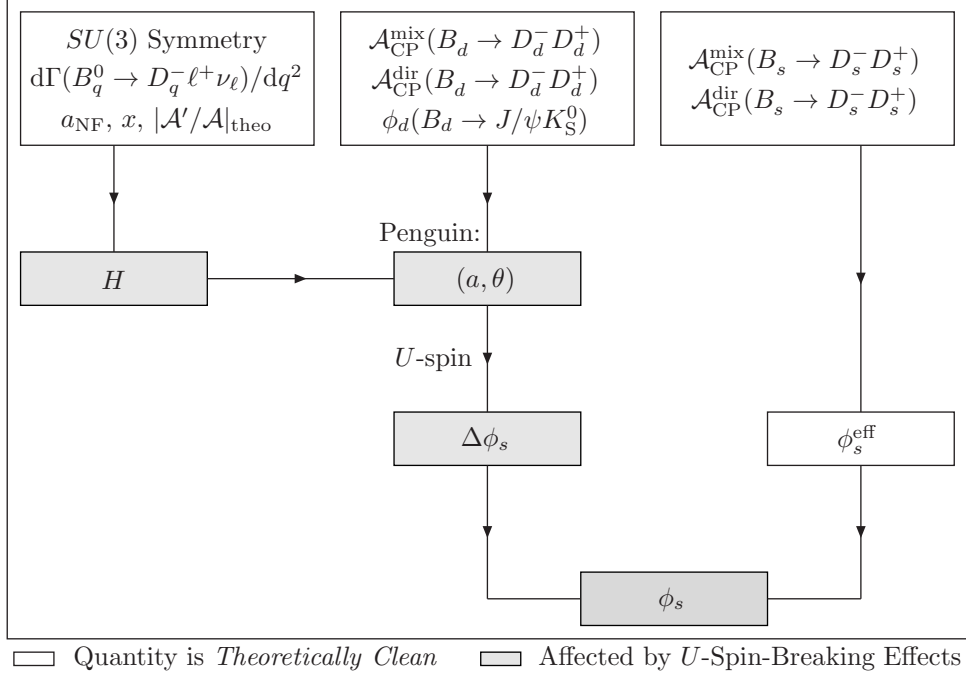


Figure 14: Flow chart illustrating the less favourable strategy to control $\Delta\phi_s$, which requires information on the H observable in addition to the $B_d^0 \rightarrow D_d^- D_d^+$ CP asymmetries.

No.	a	θ [deg]	$\mathcal{A}_{\text{CP}}^{\text{dir}}$	$\mathcal{A}_{\text{CP}}^{\text{mix}}$	H
1	0.15	260	-0.27	0.70	1.04
2	0.10	200	-0.06	0.80	1.07
3	0.25	320	-0.32	0.35	0.95
4	0.20	230	-0.26	0.82	1.12
5	0.34	216	-0.30	0.91	1.29
6	0.35	190	-0.09	0.97	1.34

Table 5: Penguin parameters and observables corresponding to the six different scenarios.

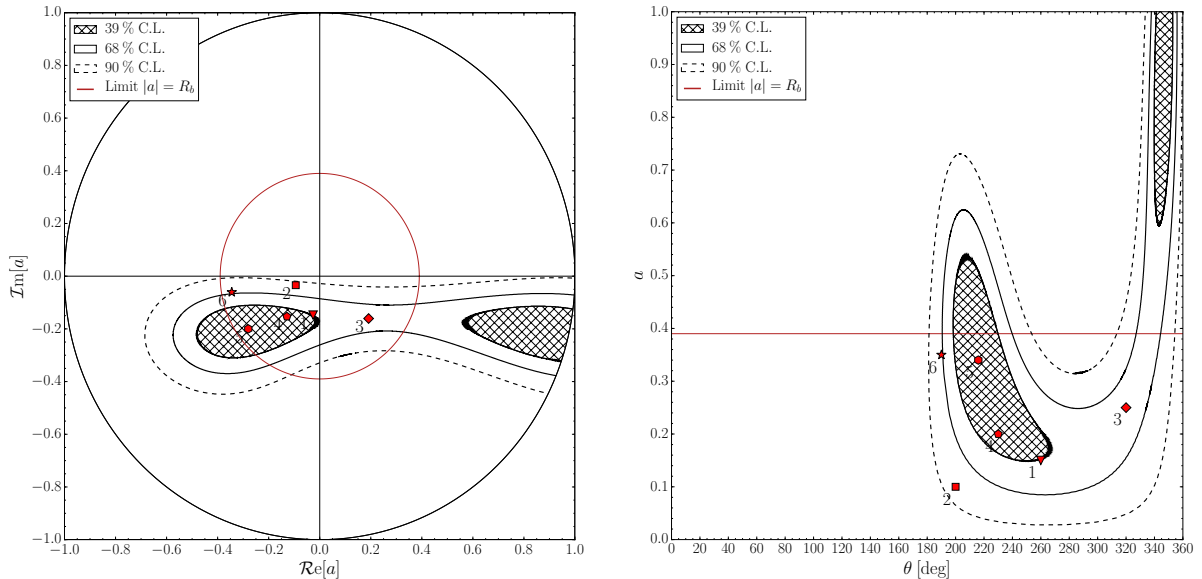


Figure 15: Distribution of six scenarios in the $\text{Re}[a]$ - $\text{Im}[a]$ plane [Left] and in the θ - a plane [Right]. Superimposed are the confidence-level contours from the fit to the current data. The red circle and horizontal line represent the natural upper limit $a = R_b$.

while the three right-most plots fall in the second category. For the three right-most plots the constraint from the mixing-induced CP asymmetry is more disk-like as the central value of $\mathcal{A}_{\text{CP}}^{\text{mix}}$ is closer to one. As a consequence, the overlap with the direct CP asymmetry, which forms a narrow band in all cases, is too large to pin down a and θ . In this respect, scenario 4 should be seen as a limiting case; information of H is not strictly necessary if one is only interested in the 1 sigma results.

For each of the six scenarios we also performed a χ^2 fit, similar to the one described in Section 3.4, but including ϕ_d as a Gaussian constraint. The fit results for a and θ , and the associated values for the shifts $\Delta\phi_d$ and $\Delta\phi_s$ are listed in Table 6. U -spin-breaking effects, parametrised by Eq. (179), have been included in the results for $\Delta\phi_s$. The associated confidence-level contours are shown in Fig. 17. In all cases we succeed in our goal of matching the foreseen experimental precision on ϕ_s , see Table 2, with an equally precise determination of $\Delta\phi_s$. This is also the case for ϕ_d^{eff} and $\Delta\phi_d$, as illustrated in Table 7. For the first three scenarios, which do not include the H observable in the fit, the resulting solution for $H_{(a,\theta)}$ and the values for the ratio of hadronic amplitudes are listed in Table 8. The resulting uncertainties are about a factor two smaller than the current theoretical uncertainties derived within the factorisation framework, and of comparable size to the experimental precision that can be obtained on the ratio of hadronic amplitudes describing the $B_d^0 \rightarrow J/\psi K_S^0$ and $B_s^0 \rightarrow J/\psi K_S^0$ decays [16]. Consequently, the experimental determination of $|\mathcal{A}'/\mathcal{A}|$ is yet another interesting topic for Belle II and the LHCb upgrade. It will provide valuable insights into possible non-factorisable U -spin-breaking effects and the hadronisation dynamics of the $B \rightarrow D\bar{D}$ decays.

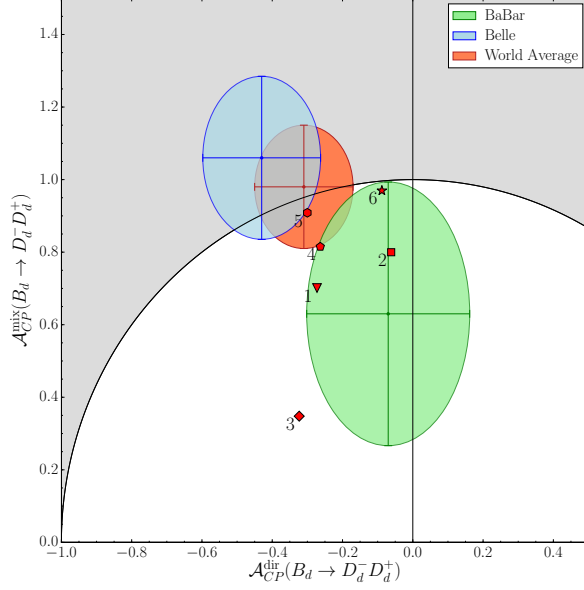


Figure 16: Distribution of the six scenarios in the $\mathcal{A}_{\text{CP}}^{\text{dir}} - \mathcal{A}_{\text{CP}}^{\text{mix}}$ plane, which can be compared to the current BaBar [Green] and Belle [Blue] measurement and the world average [Red].

No.	H	a	θ [deg]	$\Delta\phi_d$ [deg]	$\Delta\phi_s$ [deg]
1	No	$0.150^{+0.032}_{-0.029}$	$260.0^{+25.8}_{-21.8}$	$3.6^{+7.5}_{-6.3}$	$-0.15^{+0.40}_{-0.34}(\text{stat})^{+0.32}_{-0.30}(U\text{-spin})$
2	No	$0.100^{+0.079}_{-0.063}$	$200.0^{+22.1}_{-19.5}$	$10.1^{+8.9}_{-7.0}$	$-0.55^{+0.49}_{-0.39}(\text{stat})^{+0.20}_{-0.08}(U\text{-spin})$
3	No	$0.250^{+0.036}_{-0.037}$	$320.0^{+7.6}_{-7.8}$	$-21.6^{+5.8}_{-6.1}$	$1.12^{+0.24}_{-0.25}(\text{stat})^{+0.40}_{-0.40}(U\text{-spin})$
4	Yes	$0.200^{+0.063}_{-0.052}$	$230.0^{+20.8}_{-16.7}$	$14.4^{+9.8}_{-7.7}$	$-0.75^{+0.53}_{-0.42}(\text{stat})^{+0.39}_{-0.33}(U\text{-spin})$
5	Yes	$0.340^{+0.106}_{-0.087}$	$216.0^{+14.0}_{-11.5}$	$29.1^{+14.7}_{-12.1}$	$-1.62^{+0.75}_{-0.62}(\text{stat})^{+0.62}_{-0.48}(U\text{-spin})$
6	Yes	$0.350^{+0.130}_{-0.115}$	$190.0^{+6.9}_{-6.4}$	$33.6^{+15.8}_{-14.0}$	$-2.04^{+0.78}_{-0.69}(\text{stat})^{+0.56}_{-0.32}(U\text{-spin})$

Table 6: Fit results for the different scenarios.

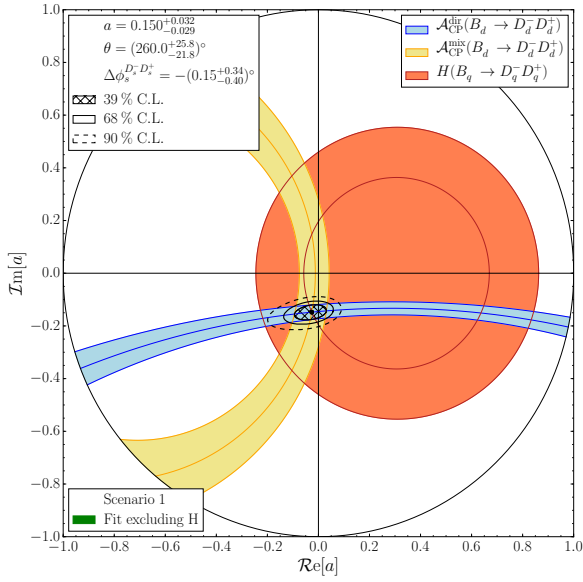
No.	ϕ_d^{eff} [deg]	$\Delta\phi_d$ [deg]
1	46.8 ± 6.9	$3.6^{+7.5}_{-6.3}$
2	53.3 ± 7.5	$10.1^{+8.9}_{-7.0}$
3	21.6 ± 5.1	$-21.6^{+5.8}_{-6.1}$
4	57.7 ± 8.8	$14.4^{+9.8}_{-7.7}$
5	72.3 ± 15.7	$29.1^{+14.7}_{-12.1}$
6	76.8 ± 19.6	$33.6^{+15.8}_{-14.0}$

Table 7: Comparison between the effective mixing phase ϕ_d^{eff} and the shift $\Delta\phi_d$.

No.	$H_{(a,\theta)}$	$ \mathcal{A}'/\mathcal{A} $
1	$1.038 \pm 0.039(a, \theta) \pm 0.002(\xi, \delta)$	1.163 ± 0.048
2	$1.067 \pm 0.053(a, \theta) \pm 0.001(\xi, \delta)$	1.179 ± 0.053
3	$0.946 \pm 0.014(a, \theta) \pm 0.002(\xi, \delta)$	1.110 ± 0.042

Table 8: Constraints on the ratio of hadronic amplitudes for those scenarios where the H observable is not needed.

Scenarios 1–3:



Scenarios 4–6:

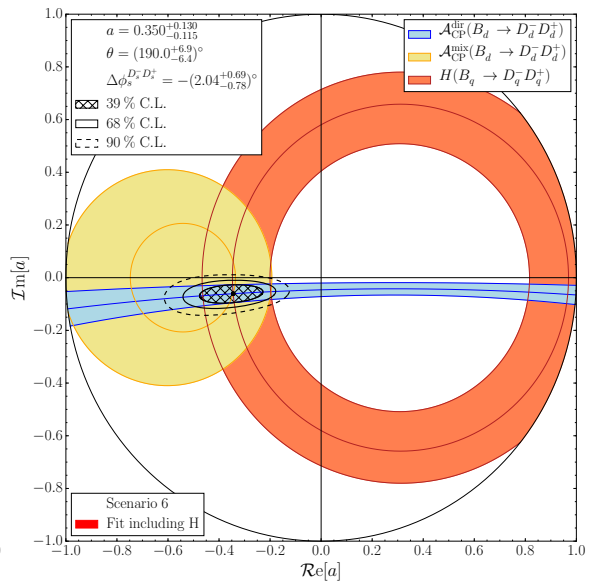
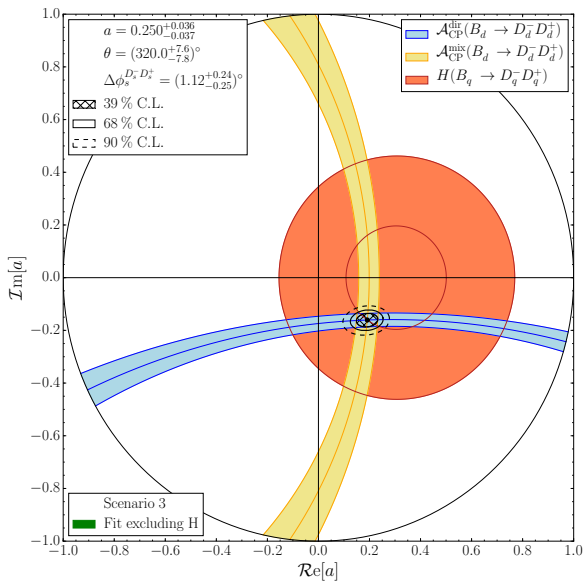
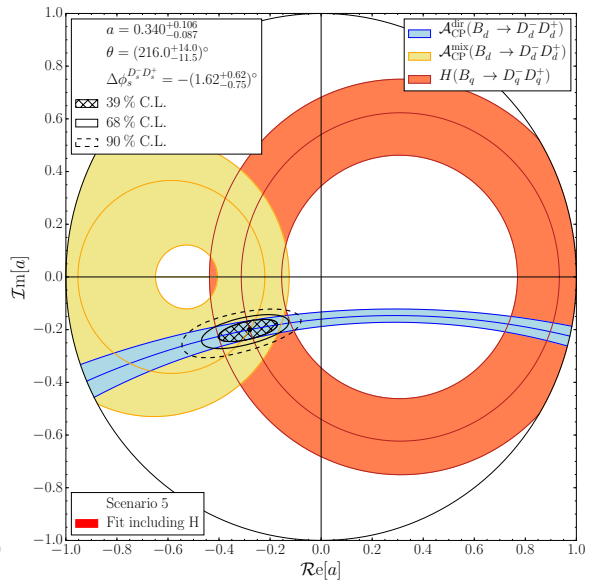
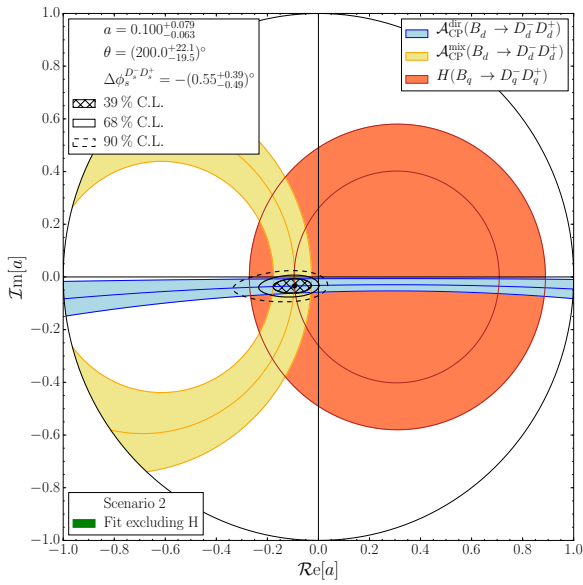
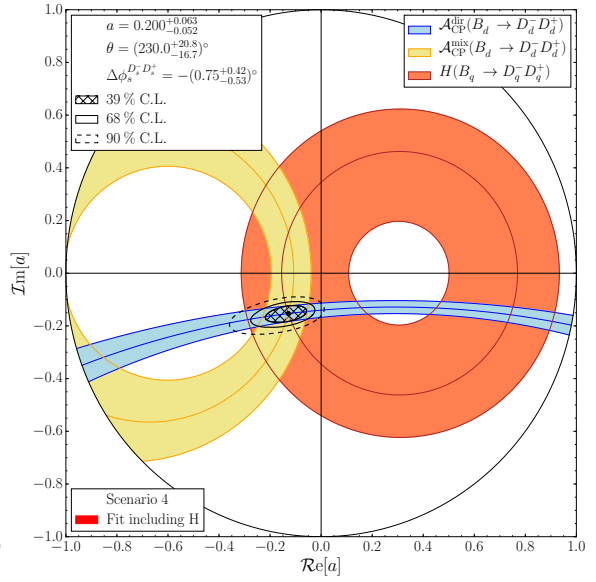


Figure 17: Illustration of the determination of the penguin parameters a and θ for the scenarios introduced above. The three left scenarios have favourable values for $\mathcal{A}_{\text{CP}}^{\text{dir}}$ – $\mathcal{A}_{\text{CP}}^{\text{mix}}$, while scenarios 5 and 6 at the right bottom would require knowledge from H .

5 Conclusions

In this paper, we have presented a detailed study of the system of $B \rightarrow D\bar{D}$ decays, exploring the picture emerging from the currently available data and proposing new strategies for the era of Belle II and the LHCb upgrade. We find that patterns in the current branching ratio measurements can be accommodated through sizeable contributions from exchange and penguin annihilation topologies, which play a more prominent role than naively expected. This feature suggests that long-distance effects of strong interactions are at work, which cannot be understood within perturbation theory.

Using data for the differential semileptonic $B_d^0 \rightarrow D_d^- \ell^+ \nu_\ell$ rate, we have determined non-factorisable contributions to the $B_d^0 \rightarrow D_d^- D_s^+$ decay, finding effects at the 25% level, including certain penguin contributions. We have pointed out that a future measurement of the semileptonic $B_s^0 \rightarrow D_s^- \ell^+ \nu_\ell$ channel would allow an optimal determination of the observable H from the $B_d^0 \rightarrow D_d^- D_d^+$ and $B_s^0 \rightarrow D_s^- D_s^+$ branching ratios, with uncertainties given only by non-factorisable U -spin-breaking corrections, which can be further quantified through the comparison of the differential $B_s^0 \rightarrow D_s^- \ell^+ \nu_\ell$ rate with the $B_s^0 \rightarrow D_s^- D_s^+$ rate. Experimental studies of the $B_s^0 \rightarrow D_s^- \ell^+ \nu_\ell$ modes are encouraged.

In view of our new insights into the prominent role of the exchange and penguin annihilation topologies, the penguin contributions may also be more important than naively expected. The current experimental situation for CP violation in the $B_d^0 \rightarrow D_d^- D_d^+$ channel is not satisfactory, with measurements of the CP-violating asymmetries by the BaBar and Belle collaborations that are not in good agreement with one another. Measurements of CP-violation in the $B_s^0 \rightarrow D_s^- D_d^+$ channel might help to clarify the situation. In the case of the $B_s^0 \rightarrow D_s^- D_s^+$ mode, the LHCb collaboration has presented a first analysis of CP violation, with large experimental uncertainties. In the future, the experimental errors can be significantly reduced. Using only information from branching ratios, we find the lower bound $a \geq 0.052$ for the penguin effects from the $B_d^0 \rightarrow D_d^- D_d^+$ and $B_s^0 \rightarrow D_s^- D_s^+$ branching ratios. Adding the current measurements of CP violation in $B_d^0 \rightarrow D_d^- D_d^+$ to the analysis, we obtain

$$a = 0.35_{-0.20}^{+0.19}, \quad \theta = (215_{-17}^{+51})^\circ, \quad \phi_d = (60_{-39}^{+43})^\circ$$

from a χ^2 fit to the data. These results indicate potentially sizeable penguin effects, although the large uncertainties do not allow us to draw further conclusions.

Since the determination of ϕ_d from $B_d^0 \rightarrow D_d^- D_d^+$ will not be competitive with the $B_d^0 \rightarrow J/\psi K_S^0$ analysis and the control of penguins through $B_s^0 \rightarrow J/\psi K_S^0$, we advocate to use ϕ_d as an input from the latter analysis for the determination of the penguin parameters from $B_d^0 \rightarrow D_d^- D_d^+$ and relating them to their counterparts in $B_s^0 \rightarrow D_s^- D_s^+$ with the help of the U -spin symmetry of strong interactions. Following these lines, it will be possible to control the penguin effects in the determination of ϕ_s from the CP violation in the $B_s^0 \rightarrow D_s^- D_s^+$ channel.

We find that the implementation of this strategy depends strongly on the values of the measured CP asymmetries, as we illustrated through a variety of future scenarios which are consistent with the current experimental situation, giving us a guideline for the LHCb upgrade era. We distinguish between two kinds of scenarios: in the first, the direct and mixing-induced CP asymmetries of the $B_d^0 \rightarrow D_d^- D_d^+$ channel are sufficient to determine a and θ in a theoretically clean way, allowing us to determine the ratio $|\mathcal{A}'|/|\mathcal{A}|$ from the observable H , providing valuable insights into non-factorisable U -spin-breaking effects. In the second — less favourable — class of scenarios, information

both from H and the CP asymmetries is needed to determine the penguin parameters. We have demonstrated that the resulting theoretical uncertainty for the penguin shift $\Delta\phi_s$ of the $B_s^0 \rightarrow D_s^- D_s^+$ channel will be smaller than the experimental uncertainty for $\phi_s^{\text{eff}}(B_s \rightarrow D_s^- D_s^+)$ in both classes of scenarios. Similar analyses can be performed for $B_d^0 \rightarrow D_d^{*-} D_d^{*+}$ and $B_s^0 \rightarrow D_s^{*-} D_s^{*+}$ decays, where time-dependent measurements of the angular distribution of the decay products of the two vector mesons are required [77, 78].

Analyses of $B \rightarrow D\bar{D}$ decays in the era of Belle II and the LHCb upgrade will offer interesting new insights both into the physics of strong interactions and into CP violation. We look forward to confronting the strategies discussed in this paper with future data!

Acknowledgements

We would like to thank Greg Ciezarek for very interesting discussions on the experimental prospects of measuring form factors with semileptonic B_s^0 decays, and Patrick Koppenburg for carefully reading the manuscript.

Appendix: Notation

In this Appendix, we give an overview of the notation, parameters and observables used in our analysis of the $B \rightarrow D\bar{D}$ system.

Var.	Eq.	Amplitude ratio	Description
a	(3)	$(P^{(ut)} + PA^{(ut)})/(T+E+P^{(ct)}+PA^{(ct)})$	Penguin contribution wrt. total ampl.
x	(43)	$(E + PA^{(ct)})(T + P^{(ct)})$	Exchange and penguin annihil. contr.
r_P	(42)	$P^{(ct)}/T$	Penguin contribution wrt. tree
r_A	(65)	$A/P^{(ut)}$	Annihilation contr. (in charged B 's)
r_{PA}	(102)	$PA^{(ut)}/P^{(ut)}$	Penguin-annihilation contribution
r_{PA}^A	(185)	$(1 + r_A)/(1 + r_{PA})$	Comparison between A and PA
$ a_{NF} ^2$	(41)	$\sim \Gamma(B \rightarrow DD')/d\Gamma(B \rightarrow D\ell\nu)/dq^2$	Non-factorisable effects
ρ	(86)		$SU(3)$ -breaking in $T+P$ contributions
ς	(115)		$SU(3)$ -breaking in $E+PA$ contributions
ξ, δ	(179)		$SU(3)$ -breaking in a and θ

Table 9: Overview of the various amplitude ratios and theoretical quantities.

Decay	Amplitude	Topologies					Variables
		T	P	E	PA	A	
$B_d^0 \rightarrow D_d^- D_d^+$	\mathcal{A}	x	x	x	x		a, x, r_P
$B_s^0 \rightarrow D_s^- D_s^+$	\mathcal{A}'	x	x	x	x		a', x', r'_P
$B_s^0 \rightarrow D_s^- D_d^+$	$\tilde{\mathcal{A}}$	x	x				\tilde{a}, \tilde{x}
$B_d^0 \rightarrow D_d^- D_s^+$	$\tilde{\mathcal{A}}'$	x	x				\tilde{a}', \tilde{x}'
$B_d^0 \rightarrow D_s^- D_s^+$	\mathcal{A}_{EPA}			x	x		x
$B_s^0 \rightarrow D_d^- D_d^+$	\mathcal{A}'_{EPA}			x	x		x'
$B^+ \rightarrow \bar{D}^0 D_d^+$	$\tilde{\mathcal{A}}_c$	x	x			x	\tilde{a}_c, r_A
$B^+ \rightarrow \bar{D}^0 D_s^+$	$\tilde{\mathcal{A}}'_c$	x	x			x	\tilde{a}'_c, r'_A

Table 10: Overview of the variables relevant to the various decays.

Decay Ratio	Observable	Eq.	Value	Used for
$B \rightarrow DD'/B \rightarrow D\ell\nu$	R_D	(33,141)		$ a_{NF} $
$B_d^0 \rightarrow D_d^- D_d^+ / B_s^0 \rightarrow D_s^- D_s^+$	H	(25)	(162)	a
$B_s^0 \rightarrow D_s^- D_d^+ / B_d^0 \rightarrow D_d^- D_s^+$	\tilde{H}	(129)	(163)	\tilde{a}
$B^+ \rightarrow \bar{D}^0 D_d^+ / B^+ \rightarrow \bar{D}^0 D_s^+$	H_c	(131)	(164)	a_c
$B_s^0 \rightarrow D_s^- D_s^+ / B_d^0 \rightarrow D_d^- D_s^+$	Ξ	(95)	(94)	\tilde{x}'
$B_d^0 \rightarrow D_d^- D_d^+ / B_s^0 \rightarrow D_s^- D_d^+$	Ξ	(105)	(104)	\tilde{x}
$B_s^0 \rightarrow D_d^- D_d^+ / B_d^0 \rightarrow D_d^- D_s^+$	Ξ	(117)	(116)	\tilde{x}'
$B_d^0 \rightarrow D_s^- D_s^+ / B_s^0 \rightarrow D_s^- D_d^+$	Ξ	(121)	(120)	\tilde{x}

Table 11: List of decay ratios and the corresponding observables and variables.

References

- [1] K. A. Olive *et al.* [Particle Data Group], *Chin. Phys. C* **38** (2014) 090001.
- [2] Y. Amhis *et al.* [Heavy Flavor Averaging Group], arXiv:1412.7515 [hep-ex]. for updates, see <http://www.slac.stanford.edu/xorg/hfag/>.
- [3] R. Aaij *et al.* [LHCb Collaboration], *Eur. Phys. J. C* **73** (2013) 4, 2373 [arXiv:1208.3355 [hep-ex]].
- [4] T. Abe *et al.* [Belle II Collaboration], arXiv:1011.0352 [physics.ins-det].
- [5] R. Fleischer, *Eur. Phys. J. C* **10** (1999) 299 [arXiv:hep-ph/9903455].
- [6] R. Fleischer, *Eur. Phys. J. C* **51** (2007) 849 [arXiv:0705.4421 [hep-ph]].
- [7] M. Gronau, J. L. Rosner and D. Pirjol, *Phys. Rev. D* **78** (2008) 033011 [arXiv:0805.4601 [hep-ph]].
- [8] R. Fleischer, *Phys. Rev. D* **60** (1999) 073008 [arXiv:hep-ph/9903540].
- [9] R. Fleischer, *Nucl. Instrum. Meth. A* **446** (2000) 1 [arXiv:hep-ph/9908340].
- [10] M. Ciuchini, M. Pierini and L. Silvestrini, *Phys. Rev. Lett.* **95** (2005) 221804 [arXiv:hep-ph/0507290]; arXiv:1102.0392 [hep-ph].
- [11] S. Faller, R. Fleischer, M. Jung, and T. Mannel, *Phys. Rev. D* **79** (2009) 014030 [arXiv:0809.0842 [hep-ph]].
- [12] S. Faller, R. Fleischer and T. Mannel, *Phys. Rev. D* **79** (2009) 014005 [arXiv:0810.4248 [hep-ph]].
- [13] M. Gronau and J. L. Rosner, *Phys. Lett. B* **672** (2009) 349 [arXiv:0812.4796 [hep-ph]].
- [14] M. Jung, *Phys. Rev. D* **86** (2012) 053008 [arXiv:1206.2050 [hep-ph]].
- [15] X. Liu, W. Wang and Y. Xie, *Phys. Rev. D* **89** (2014) 094010 [arXiv:1309.0313 [hep-ph]].
- [16] K. De Bruyn and R. Fleischer, *JHEP* **1503** (2015) 145 [arXiv:1412.6834 [hep-ph]].
- [17] P. Frings, U. Nierste and M. Wiebusch, arXiv:1503.00859 [hep-ph].
- [18] S. Okubo, *Phys. Lett.* **5** (1963) 165.
- [19] G. Zweig, CERN-TH-412, NP-8419 (1964).
- [20] J. Iizuka, *Prog. Theor. Phys. Suppl.* **37** (1966) 21.
- [21] R. Fleischer, *Int. J. Mod. Phys. A* **12** (1997) 2459 [arXiv:hep-ph/9612446].
- [22] R. Fleischer and T. Mannel, *Phys. Lett. B* **506** (2001) 311 [arXiv:hep-ph/0101276].
- [23] A. J. Buras, R. Fleischer, S. Recksiegel and F. Schwab, *Phys. Rev. Lett.* **92** (2004) 101804 [arXiv:hep-ph/0312259].

- [24] A. J. Buras, R. Fleischer, S. Recksiegel and F. Schwab, Nucl. Phys. B **697** (2004) 133 [arXiv:hep-ph/0402112].
- [25] R. Fleischer, S. Jäger, D. Pirjol and J. Zupan, Phys. Rev. D **78** (2008) 111501 [arXiv:0806.2900 [hep-ph]].
- [26] V. Barger, L. Everett, J. Jiang, P. Langacker, T. Liu and C. Wagner, Phys. Rev. D **80** (2009) 055008 [arXiv:0902.4507 [hep-ph]].
- [27] V. Barger, L. L. Everett, J. Jiang, P. Langacker, T. Liu and C. E. M. Wagner, JHEP **0912** (2009) 048 [arXiv:0906.3745 [hep-ph]].
- [28] N. Cabibbo, Phys. Rev. Lett. **10** (1963) 531.
- [29] M. Kobayashi and T. Maskawa, Prog. Theor. Phys. **49** (1973) 652.
- [30] M. Gronau, O. F. Hernandez, D. London and J. L. Rosner, Phys. Rev. D **52** (1995) 6356 [arXiv:hep-ph/9504326].
- [31] L. Wolfenstein, Phys. Rev. Lett. **51** (1983) 1945.
- [32] J. Charles, O. Deschamps, S. Descotes-Genon, H. Lacker, A. Menzel, S. Monteil, V. Niess and J. Ocariz *et al.*, arXiv:1501.05013 [hep-ph]; for updates, see <http://ckmfitter.in2p3.fr>.
- [33] R. Fleischer, Phys. Rept. **370** (2002) 537 [arXiv:hep-ph/0207108].
- [34] M. Bander, D. Silverman and A. Soni, Phys. Rev. Lett. **43** (1979) 242.
- [35] R. Fleischer, Z. Phys. C **58** (1993) 483.
- [36] R. Fleischer, Z. Phys. C **62** (1994) 81.
- [37] A. J. Buras, R. Fleischer and T. Mannel, Nucl. Phys. B **533** (1998) 3 [arXiv:hep-ph/9711262].
- [38] I. Dunietz, R. Fleischer and U. Nierste, Phys. Rev. D **63** (2001) 114015 [arXiv:hep-ph/0012219].
- [39] K. De Bruyn, R. Fleischer, R. Kneijens, P. Koppenburg, M. Merk and N. Tuning, Phys. Rev. D **86** (2012) 014027 [arXiv:1204.1735 [hep-ph]].
- [40] R. Aaij *et al.* [LHCb Collaboration], Phys. Rev. Lett. **112** (2014) 11, 111802 [arXiv:1312.1217 [hep-ex]].
- [41] R. Fleischer and T. Mannel, Phys. Rev. D **57** (1998) 2752 [arXiv:hep-ph/9704423].
- [42] R. Fleischer and S. Recksiegel, Phys. Rev. D **71** (2005) 051501 [arXiv:hep-ph/0409137].
- [43] J. D. Bjorken, Nucl. Phys. Proc. Suppl. **11** (1989) 325.
- [44] D. Bortoletto and S. Stone, Phys. Rev. Lett. **65** (1990) 2951.
- [45] J. L. Rosner, Phys. Rev. D **42** (1990) 3732.

- [46] M. Neubert and B. Stech, Adv. Ser. Direct. High Energy Phys. **15** (1998) 294 [arXiv:hep-ph/9705292].
- [47] M. Beneke, G. Buchalla, M. Neubert and C. T. Sachrajda, Nucl. Phys. B **591** (2000) 313 [arXiv:hep-ph/0006124].
- [48] R. Fleischer, N. Serra and N. Tuning, Phys. Rev. D **83** (2011) 014017 [arXiv:1012.2784 [hep-ph]].
- [49] A. J. Buras, Nucl. Phys. B **434** (1995) 606 [arXiv:hep-ph/9409309].
- [50] R. Fleischer, N. Serra and N. Tuning, Phys. Rev. D **82** (2010) 034038 [arXiv:1004.3982 [hep-ph]].
- [51] R. Fleischer, Nucl. Phys. B **412** (1994) 201.
- [52] J. L. Rosner and S. Stone, arXiv:1309.1924 [hep-ex].
- [53] S. Aoki *et al.* [Flavour Lattice Averaging Group], Eur. Phys. J. C **74** (2014) 9, 2890 [arXiv:1310.8555 [hep-lat]].
- [54] M. Neubert and V. Rieckert, Nucl. Phys. B **382** (1992) 97.
- [55] M. Neubert, Nucl. Phys. B **371** (1992) 149.
- [56] A. Abd El-Hady, A. Datta, K. S. Gupta and J. P. Vary, Phys. Rev. D **55** (1997) 6780 [arXiv:hep-ph/9605397].
- [57] J.A. Bailey *et al.* [Fermilab Lattice and MILC Collaborations], arXiv:1503.07237 [hep-lat].
- [58] H. Na, C. M. Bouchard, G. P. Lepage, C. Monahan and J. Shigemitsu, arXiv:1505.03925 [hep-lat].
- [59] R. Aaij *et al.* [LHCb Collaboration], arXiv:1504.01568 [hep-ex], submitted to Nature Physics.
- [60] A. Bevan, *et al.* [UTfit Collaboration], arXiv:1411.7233 [hep-ph]; for updates, see <http://www.utfit.org>.
- [61] R. Aaij *et al.* [LHCb Collaboration], Phys. Rev. D **87** (2013) 9, 092007 [arXiv:1302.5854 [hep-ph]].
- [62] E. Jenkins and M.J. Savage, Phys. Lett. B **281** (1992) 331.
- [63] B. Grinstein, E. E. Jenkins, A. V. Manohar, M. J. Savage and M. B. Wise, Nucl. Phys. B **380** (1992) 369 [arXiv:hep-ph/9204207].
- [64] A. X. El-Khadra, PoS LATTICE **2013** (2014) 001 [arXiv:1403.5252 [hep-lat]].
- [65] J. A. Bailey *et al.*, [Fermilab Lattice and MILC Collaborations] Phys. Rev. D **85** (2012) 114502 [Erratum-ibid. D **86** (2012) 039904] [arXiv:1202.6346 [hep-lat]].
- [66] M. Gronau, O. F. Hernandez, D. London and J. L. Rosner, Phys. Rev. D **50** (1994) 4529 [arXiv:hep-ph/9404283].

- [67] B. Aubert *et al.* [BaBar Collaboration], Phys. Rev. D **79** (2009) 032002 [arXiv:0808.1866 [hep-ex]].
- [68] M. Röhrken *et al.* [Belle Collaboration], Phys. Rev. D **85** (2012) 091106 [arXiv:1203.6647 [hep-ex]].
- [69] R. Aaij *et al.* [LHCb Collaboration], Phys. Rev. Lett. **113** (2014) 21, 211801 [arXiv:1409.4619 [hep-ex]].
- [70] M. Jung and S. Schacht, Phys. Rev. D **91** (2015) 3, 034027 [arXiv:1410.8396 [hep-ph]].
- [71] G. Majumder *et al.* [Belle Collaboration], Phys. Rev. Lett. **95** (2005) 041803 [arXiv:hep-ex/0502038].
- [72] I. Adachi *et al.* [Belle Collaboration], Phys. Rev. D **77** (2008) 091101 [arXiv:0802.2988 [hep-ph]].
- [73] A. Zupanc *et al.* [Belle Collaboration], Phys. Rev. D **75** (2007) 091102 [arXiv:hep-ex/0703040].
- [74] G. Huang [BESIII Collaboration], arXiv:1209.4813 [hep-ph].
- [75] D. M. Asner *et al.* [BESIII Collaboration], Int. J. Mod. Phys. A **24** (2009) S1 [arXiv:0809.1869 [hep-ph]].
- [76] A. Zupanc *et al.* [Belle Collaboration], JHEP **1309** (2013) 139 [arXiv:1307.6240 [hep-ph]].
- [77] R. Fleischer and I. Dunietz, Phys. Rev. D **55** (1997) 259 [arXiv:hep-ph/9605220].
- [78] A. S. Dighe, I. Dunietz and R. Fleischer, Eur. Phys. J. C **6** (1999) 647 [arXiv:hep-ph/9804253].